Geosci. Model Dev. Discuss., https://doi.org/10.5194/gmd-2018-144
Manuscript under review for journal Geosci. Model Dev.
Discussion started: 12 July 2018

Geoscientific Model Development Discussions
Open Access
EGU

Ensemble Forecasts of Air Quality in Eastern China

Part 1. Model Description and Implementation of the MarcoPolo-Panda Prediction System

Guy P. Brasseur
Max Planck Institute for Meteorology, Hamburg, Germany
and National Center for Atmospheric Research, Boulder, CO, USA

Ying Xie
Shanghai Meteorological Service, Shanghai, China

A. Katinka Petersen
Max Planck Institute for Meteorology, Hamburg, Germany

Idir Bouarar
Max Planck Institute for Meteorology, Hamburg, Germany

Johannes Flemming
European Centre for Middle Range Weather Forecasts, Reading, UK.

Michael Gauss
Norwegian Meteorological Institute, Oslo, Norway

Fei Jiang
Nanjing University, Nanjing, China

Rostislav Kouznetsov
Finnish Meteorological Institute, Helsinki, Finland.

Richard Kranenburg
TNO, Utrecht, The Netherlands

Bas Mijling
Royal Netherlands Meteorological Institute (KNMI), De Bilt, The Netherlands

Vincent-Henri Peuch
European Centre for Middle Range Weather Forecasts, Reading, UK

Matthieu Pommier
Norwegian Meteorological Institute, Oslo, Norway

Arjo Segers
TNO, Utrecht, The Netherlands

Mikhail Sofiev
Finnish Meteorological Institute, Helsinki, Finland

Renske Timmermans
TNO, Utrecht, The Netherlands

Ronald van der A
Royal Netherlands Meteorological Institute (KNMI), De Bilt, The Netherlands,
and Nanjing University of Information Science and Technology, Nanjing, China

Stacy Walters
National Center for Atmospheric Research, Boulder, CO, USA

Jianming Xu
Shanghai Meteorological Service, Shanghai, China

Guangqiang Zhou
Shanghai Meteorological Service, Shanghai, China

Geosci. Model Dev. Discuss., https://doi.org/10.5194/gmd-2018-144
Manuscript under review for journal Geosci. Model Dev.
Discussion started: 12 July 2018

Geoscientific Model Development Discussions

64 **Abstract**
65
66 An operational multi-model forecasting system for air quality including 9 different chemical
67 transport models has been developed and is providing daily forecasts of ozone, nitrogen
68 oxides, and particulate matter for the 37 largest urban areas of China (population higher
69 than 3 million in 2010). These individual forecasts as well as the mean and median
70 concentrations for the next 3 days are displayed on a publicly accessible web site
71 (www.marcopolo-panda.eu). The paper describes the forecasting system and shows some
72 selected illustrative examples of air quality predictions. It presents an inter-comparison of
73 the different forecasts performed during a given period of time (1-15 March 2017), and
74 highlights recurrent differences between the model output as well as systematic biases that
75 appear in the median concentration values. Pathways to improve the forecasts by the multi-
76 model system are suggested.
77
78
79

Geosci. Model Dev. Discuss., https://doi.org/10.5194/gmd-2018-144
Manuscript under review for journal Geosci. Model Dev.
Discussion started: 12 July 2018

Geoscientific Model Development Discussions

1. Introduction

The rapid economic growth in China has been accompanied with a substantial degradation of air quality, particularly in the densely populated areas of the eastern part of the country. Air pollution is the source of cardiovascular and respiratory illness, increased stress to heart and lungs and cell damage in the respiratory system, which in turn can result in fatalities resulting from ischemic heart disease, chronic obstructive pulmonary disease (COPD) and Lower Respiratory Infections. To address this problem, China is taking effective measures to reduce the emission of primary pollutants such as nitrogen oxides (NOx), volatile organic compounds (VOCs) and particulate matter (PM). In addition to these long-term mitigation measures, immediate action can be taken to avoid the occasional occurrence of acute air pollution episodes, particularly in winter during stable meteorological situations, by drastically reducing emissions associated with polluting activities during the periods of predicted events. The implementation of such measures requires that accurate forecasts of air quality be produced and made available to local and regional authorities. Alerts to warn the public of the imminence of acute pollution episodes can be released several days before the event on the basis of model predictions.

Advanced forecast models include a detailed formulation of the chemical and physical processes responsible for the formation of secondary pollutants such as ozone and particulate matter in response to the emissions of primary species produced as a result of industrial, agricultural and residential activities, energy production and transportation. These models simulate the transport of these constituents by the atmospheric circulation as well as vertical exchanges by convective motions and turbulent boundary layer mixing. Meteorological information provided by weather forecast models is therefore an essential input to regional air quality models. Surface deposition of oxidized compounds and wet scavenging of soluble species are also taken into account. The atmospheric concentrations of the chemical and physically interacting species are obtained by solving a mathematically stiff system of partial differential equations with appropriate initial and boundary conditions.

The approach used to produce predictions of air quality bears a lot of resemblance with the methods used for weather forecasts. In both cases, models make use of similar numerical algorithms, include assimilated data, produce large amounts of output that have to be analysed and evaluated, and eventually disseminated to the public in the form of easily accessible information. The steady progress made in the numerical weather prediction since the 1980's (Bauer et al., 2015), through combined scientific, computational and observational advances, has also considerably improved our capability of providing predictive information on air quality and on its impacts for human society (i.e., health, food production and the state of ecosystems).

Many models are available for operationally forecasting air quality [Kukkonen et al., 2012] and have been tested in different contexts. These models are usually driven by different input data (surface emissions, weather forecasts, chemical schemes, aerosol formulation, land use data, boundary conditions, etc.) and hence generate different output (e.g., different concentrations of chemical species). In most cases, it is difficult to clearly

distinguish between models that perform well and models that perform poorly because the success of individual models varies with the conditions that are encountered (e.g., geographic location, season, meteorological situation) and can be different for the different chemical species and for different statistical parameters. If the models involved have been developed rather independently from each other their results can be combined and their individual behaviours can be examined by comparing the predicted fields to the median or the mean derived from the ensemble of simulations. Much can be learned from a systematic day-by-day examination of the model behaviour operated in a forecast mode.

Building ensemble of models is an attractive approach to forecast air quality, because the inter-model variability provides insight on the robustness of the results or conversely on their uncertainties [Vautard et al., 2006; Solazzo et al., 2012]. Further, the composite products have usually better overall performance than the results produced by individual systems [Galmarini et al., 2013; Riccio et al., 2007; Sofiev, 2015; 2017]. This approach is especially useful in the context of decision-making since it samples the uncertainty space associated with the different individual forecasts.

Numerical weather and seasonal forecasting are usually based on a single model ensemble in which the initial conditions are slightly perturbed so that different likely evolutions of the atmospheric dynamics can be projected. In the case of air quality forecasts, which are not only initial value problems, it is advisable to also perturb emissions, meteorology and boundary conditions as well as model parameters (kinetic reaction rates…), which is best performed by considering a multi-model ensemble [Dabberdt and Miller, 2000]. Nevertheless, in addition, it would also be useful to assess the behaviour of a single air quality model that is driven by different realizations of ensemble meteorological forecasts.

The models used in the present study have been developed rather independently, and this leads to a rather broad range of model results. Model performance does not only depend on the quality of emissions datasets: they differ for a wide range of reasons, including dynamical and weather aspects but also the adopted formulation (parameterisations, operator splitting, time integration…) and numerical algorithms. An inspection of the different choices made in the models can lead to some improvements in model configurations, and hence will reduce the “artificial” spread between calculated fields. This spread often results from errors in the configuration (set-up bugs…) or from inaccuracies in the adopted input parameters (land-use…). By including each model configuration within a large ensemble, the combined performance of the forecast system is considerably less affected by initial implementation issues or inadequate choice of input parameters applied in individual models.

This paper describes the early phase of a system that forecasts air quality in eastern China. The system can be characterized as a multi-model “ensemble of opportunity” (as defined by a combination of models running in their default configurations) that is evolving into an operational air quality ensemble prediction system, similar to the system established in Europe under the Copernicus Atmospheric Monitoring Service (CAMS) [Marecal et al., 2015]. The concept adopted here will be briefly presented in Section 2. Section 3 presents a description of the different models and Section 4 discusses the performance of the whole

system and of the contributing models. Approaches to improve the performance of the system are presented in Section 5.

The ensemble of models considered in the present study has been assembled under the Panda and MarcoPolo projects supported by the European Commission within the Framework Programme 7 (FP7). Seven models were initially included in the operational system: the global IFS model developed and operated by the European Centre for Middle Range Weather Forecasts (ECMWF), five regional models implemented by European research and service institutions (CHIMERE by the Royal Netherlands Meteorological Institute (KNMI), WRF-Chem-MPIM by the Max Planck Institute for Meteorology (MPIM), SILAM by Finnish Meteorological Institute (FMI), EMEP/MSC-W by the Norwegian Meteorological Institute (MET.Norway), LOTOS-EUROS by The Netherlands Organisation for Applied Scientific Research (TNO)), and one model (WRF-Chem-SMS) applied in China by the Shanghai Meteorological Service (SMS). In later steps, forecasts by additional regional models applied by Nanjing University (WRF-CMAQ) and by the Shanghai Meteorological Service (WARMS-CMAQ) were added to the ensemble. In the following Section, we provide a brief overview of these different models. Only seven of them contribute to the inter-comparison presented in Section 4.

2. Description of the Models included in the Ensemble

In the following subsections, each of the 9 participating models will be described. Table 2a-b presents the key characteristics of each model involved in the inter-comparison and Table 3 summarizes the emissions adopted in each model.

2.1. IFS

IFS (Integrated Forecasting System) is ECMWF's global Numerical Weather Prediction system. As part of the past series of European projects MACC and now of CAMS, the Copernicus Atmosphere Monitoring Service, IFS has been developed to represent optionally chemical processes in the troposphere and in the stratosphere. Flemming et al. (2015) provide a detailed description of the modelling of chemical processes in the IFS, and Inness et al. (2015) describe the aata assimilation aspects.

For the work presented here, the version of IFS used is Cycle 43R1 (see documentation at https://www.ecmwf.int/en/forecasts/documentation-and-support/changes-ecmwf-model/ifs-documentation). The model is run globally at a resolution of T511 (about 40km) on the horizontal, and with 60 levels on the vertical extending up to the top of the stratosphere. The chemical package used originates from the TM5 Chemistry and Transport Model (Huijnen et al., 2010). It has been fully integrated into the IFS code and comprises 54 tracers and 120 reactions focusing on tropospheric ozone-CO-NMVOC chemistry. In the configuration used here, stratospheric ozone is modelled with a simple linearized scheme. Aerosols are represented using the scheme described by Morcrette et al. (2009), which includes 5 species: dust, sea-salt, black carbon, organic carbon and sulphates. Tracers are transported using the semi-Lagrangian scheme available in IFS with a mass fixer activated in order to minimise mass non-conservation.

During the study period, IFS has been run twice daily (5-day forecasts) assimilating a range of satellite chemical data on top of the full list of meteorological satellite and non-satellite data that ECMWF uses for its medium-range weather forecasts. Table 1 indicates the satellite data streams actively assimilated for the experiments presented here. As a result, IFS forecasts benefit from all these observations to afford a realistic representation of large scales for weather parameters as well as, to some extent, for chemical variables (species assimilated).

IFS used the MACCITY emission data set updated for the year 2017. Biogenic emissions of VOC were taken from a climatology of a multi-year MEGAN model simulation. Daily emissions from biomass burning were derived from satellite retrieval of fire radiative power (FRP) from the MODIS instruments by the Global Fire Assimilation System (GFAS, Kaiser et al. 2012). The observed fire emissions from the day before the forecast start are used for all five days of the forecast. Desert dust and sea salt emissions were simulated online for each time step based on the IFS meteorological fields and the land use.

As part of CAMS, the chemical configuration of IFS benefits from routine detailed evaluations. Validation reports are produced quarterly and can be found here (http://atmosphere.copernicus.eu/quarterly_validation_reports). The report for the period March-May 2017 provides insight on the overall performance of the runs that are also presented here. Further information about the IFS code can be obtained from Vincent Henri Peuch vincent-henri.peuch@ecmwf.int and on the web site https://www.ecmwf.int/en/about/what-we-do/environmental-services/copernicus-atmosphere-monitoring-service

Table 1. Satellite data streams (atmospheric composition variables only) assimilated in IFS.

Instrument	Satellite	Space Agency	Data Provider	Species
MODIS	EOS-Aqua, EOS-Terra	NASA	NASA	AOD
MLS	EOS-Aura	NASA		O3 profile
OMI	EOS-Aura	NASA	KNMI	O3, NO2, SO2
SBUV-2	NOAA-19	NOAA	NOAA	O3 profile
IASI	METOP-A, METOP-B	EUMETSAT/CNES	ULB/LATMOS	CO
MOPITT	EOS-Terra	NASA	NCAR	CO
GOME-2	METOP-A, METOP-B	EUMETSAT/ESA	AC-SAF	O3, SO2
OMPS	Suomi-NPP	NOAA	EUMETSAT	O3
PMAp	METOP-A, METOP-B	EUMETSAT	EUMETSAT	AOD

2.2. CHIMERE

CHIMERE is a regional chemistry-transport model used for analysis, scenarios and forecast (Menut et al., 2013). When used in the forecast mode, the model provides local scale information (to be compared with data from numerous air quality networks), or regional scale information (e.g., the French PREVAIR and the Copernicus CAMS systems). CHIMERE is

an open-source model, freely distributed at www.lmd.polytechnique.fr/chimere. In this version, CHIMERE is used in off-line mode, forced by pre-calculated hourly meteorological fields for the dynamics and by several emissions fluxes for the chemistry. The emissions are pre-calculated or on-line estimated in the model with anthropogenic emissions (MEIC 2010), biogenic emissions with the online model of emissions of gases and aerosols from nature (MEGAN, Guenther et al., 2006), mineral dust (Menut et al., 2013) and biomass burning emissions (Turquety et al., 2014). The gas phase chemistry is calculated using the MELCHIOR2 mechanism and the aerosols are represented using a distribution of 10 bins, from 40nm to 40µm to well describe both number and mass. The chemical boundary conditions are provided by the LMDz-INCA model for gas and particles (Szopa et al., 2009), except for mineral dust extracted from global GOCART simulations (Ginoux et al., 2001). Further information about the implementation of the model for air quality forecasts in China can be obtained from Ronald van der A (avander@knmi.nl) at KNMI and on the web site http://www.lmd.polytechnique.fr/chimere/CW-download.php .

2.3. WRF-Chem-MPIM

The Weather Research and Forecasting model coupled to chemistry (WRF-Chem) is a mesoscale non-hydrostatic meteorological model (Skamarock et al., 2008) coupled "online" with chemistry that simultaneously predicts meteorological and chemical components of the atmosphere (Grell et al., 2005; Fast et a., 2006).

WRF-Chem-MPIM is based on version 3.6.1 of the WRF-Chem model coupled to the gas phase chemistry and the aerosol microphysics schemes provided by the Model for Ozone and Related Chemical Tracers (MOZART-4, Emmons et al., 2010) and the Model for Simulating Aerosol Interactions and Chemistry (MOSAIC, Zaveri et al., 2008), respectively. Aerosols sizes are represented by four consecutive bins, and the formation of secondary organic aerosol (SOA) from anthropogenic precursors is parameterized according to Hodzic and Jimenez (2011).

Two nested model domains with horizontal resolutions of 60 km (Asian continent from India to Japan) and 20 km (eastern China), respectively are implemented. The vertical grid is composed of 51 levels extending from the surface to 10 hPa (~30 km). A more complete description of the selected physical and chemical options is provided in the WRF and in the WRF-Chem user's guides under
http://www2.mmm.ucar.edu/wrf/users/docs/user_guide_V3.6/ARWUsersGuideV3.6.1.pdf
and https://ruc.noaa.gov/wrf/wrf-chem/Users_guide.pdf.

The WRF-Chem-MPIM model forecasts are initialized and forced at the lateral boundaries every day by 6 hourly meteorological analysis data from the NCEP Global Forecast System (GFS) at 0.5 degree resolution. For the chemical and aerosol species, 6 hourly datasets are provided by the global operational forecasting system implemented within the Copernicus Atmospheric Monitoring Service project (Flemming et al., 2015). More information on the model's configuration can be obtained from Idir Bouarar (idir.bouarar@mpimet.mpg.de) at the Max Planck Institute for Meteorology and on the web site http://www2.mmm.ucar.edu/wrf/users/downloads.html.

Geosci. Model Dev. Discuss., https://doi.org/10.5194/gmd-2018-144
Manuscript under review for journal Geosci. Model Dev.
Discussion started: 12 July 2018

2.4. SILAM

FMI uses the SILAM model version 5.5 (Sofiev et al., 2015). SILAM includes a meteorological pre-processor for diagnosing the basic features of the boundary layer and the free troposphere from the meteorological fields provided by various meteorological models (Sofiev et al., 2010). The dry deposition scheme for particles is described in Kouznetsov and Sofiev (2012). The surface resistance model for gases is based on a modified Wesely scheme (Wesely, 1989).

The gas phase chemistry was simulated with CBM-IV, with reaction rates updated according to the recommendations of IUPAC (http://iupac.pole-ether.fr) and JPL (http://jpldataeval.jpl.nasa.gov) and the terpenes oxidation added from CB05 reaction list (Yarwood et al., 2005). The sulphur chemistry and secondary inorganic aerosol formation is computed with an updated version of the DMAT scheme (Sofiev, 2000) and secondary organic aerosol formation with the Volatility Basis Set (VBS, Donahue et al., 2006), the volatility distribution of anthropogenic OC taken from Shrivastava et al. (2011).

The MACCITY land-based emissions are used together with STEAM shipping emissions. The simulations include sea-salt emissions as in Sofiev et al. (2011), biogenic VOC (volatile organic compounds) emissions as in Poupkou et al. (2010) and wild-land fire emissions as in Soares et al. (2015) and desert dust.

The grid cell size was roughly 15km × 10km (0.125° × 0.125°) covering the whole China, India, Japan and several countries of South-East Asia (67E, 7N) – (147E, 54N). The Asian forecasts are nested into the SILAM global AQ forecasts (http://silam.fmi.fi), from where they take lateral and top boundary conditions. The initial conditions for each run are taken from the previous-day forecast or, in case of failure, from global computations. Detailed information about the SILAM modelling system can be obtained from Mikhail Sofiev (Mikhail.Sofiev@fmi.fi) and from Rostislav Kouznetsov (rostislav.kouznetsov@fmi.fi) and on the web site of the Finnish Meteorological Institute (http://silam.fmi.fi/).

2.5. EMEP

The EMEP/MSC-W model (hereafter referred to as 'EMEP model') is a 3-D Eulerian Chemical Transport Model described in detail in Simpson et al. (2012). Although the model has traditionally been aimed at European simulations, global modelling has been possible for many years (Jonson et al., 2010; Wild et al., 2012). The EMEP configuration for the present study covers the East-Asian domain [15°N-55°N] x [90°E-135°E] with a horizontal resolution of 0.1° x 0.1° (longitude-latitude). The model uses 20 vertical levels defined as sigma coordinates. The 10 lowest levels are within the PBL, and the top of the model domain is at 100 hPa.

Particulate (PM) emissions are split into elementary carbon (EC), organic matter (OM) (here assumed inert) and the remainder, for both fine and coarse PM. The OM emissions are further divided into fossil fuel and wood-burning compounds for each source sector. As in Bergström et al. (2012), the Organic Matter/Organic Carbon ratio of emissions by mass is assumed to be 1.3 for fossil-fuel sources and 1.7 for wood-burning sources. The model also

calculates windblown dust emissions from soil erosion. Secondary PM2.5 aerosol consists of inorganic sulphate, nitrate and ammonium, and SOA; the latter is generated from both anthropogenic and biogenic emissions (anthropogenic SOA and biogenic SOA respectively), using the 'VBS' scheme detailed in Bergström et al (2012) and Simpson et al (2012).

Model updates since Simpson et al. (2012), resulting in EMEP model version rv4.9 as used here, have been described in Simpson et al. (2016) and references cited therein. The main changes concern a new calculation of aerosol surface area, revised parameterizations of N_2O_5 hydrolysis on aerosols, additional gas-aerosol loss processes for O_3, HNO_3 and HO_2, a new scheme for ship NO_x emissions, and the use of new maps for global leaf-area (used to calculate biogenic VOC emissions) – see Simpson et al. (2015) for details. The EMEP model, including a user guide, is publicly available as Open Source code at https://github.com/metno/emep-ctm. For more details, please contact Michael Gauss (michael.gauss@met.no).

The EMEP forecasts are driven by 3-hourly meteorological forecast data from the ECMWF IFS model at 0.1 degree resolution. As for WRF-Chem, 6-hourly datasets for the chemical and aerosol species are provided by the global operational forecasting system implemented within the Copernicus Atmospheric Monitoring Service project.

2.6. LOTOS-EUROS

LOTOS-EUROS is a three-dimensional regional chemistry transport model (CTM) for simulation of trace gases and aerosol concentrations in the boundary layer. Meteorological input is obtained from an offline model, in this study from ECMWF. The model is of intermediate complexity allowing long-term model simulations. For a detailed model description we refer to Manders et al. (2017) and references therein.

In this study LOTOS-EUROS version 1.10 was used to simulate air quality over China. The configuration is described by Timmermans et al. (2017) who adopted this version of the model to investigate the origin of fine particulate matter across China using a source apportionment technique. Through a one-way nesting procedure a simulation over East-China was performed on a resolution of 0.25° longitude by 0.125° latitude, approximately 21 by 15 km^2. This domain is nested in a larger domain covering China almost entirely with a resolution 1° longitude by 0.5° latitude, approximately 84 by 56 km^2. Chemical boundary conditions for the coarse resolution domain were taken from the CAMS global modelling framework (Flemming et al., 2015) and include trace gasses and aerosols. In the vertical, the model used a boundary layer approach with 5 layers: a surface layer of 25m, a well-mixed boundary layer, two reservoir layers, and a layer for the free troposphere. The boundary layer height therefore defines the vertical structure of the model, and is here taken from the meteorological input. More details about the code can be obtained by contacting Renske Timmermans (renske.timmermans@tno.nl) at TNO or by consulting the web site https://lotos-euros.tno.nl/.

2.7. WRF-Chem-SMS

WRF-Chem-SMS is based on WRF-Chem (Grell et al., 2005) version 3.2. The Regional Acid Deposition Model version 2 (RADM2, Chang et al., 1989) is used to represent gas-phase chemistry. ISORROPIA II is implemented to treat thermodynamic equilibrium for inorganic aerosols (Fountoukis and Nenes, 2007), and the Secondary ORGanic Aerosol Model (SORGAM) (Schell et al., 2001) is used to parameterize secondary organic aerosol formation. Madronich TUV scheme is applied for photolysis (Madronich and Flocke, 1999; Tie et al., 2003). The model domain covers the eastern region of China with horizontal resolutions of 6 km and 28 vertical layers. Biogenic emissions are calculated online using MEGAN model (Guenther et al., 2012). The multi-resolution emission inventory for China (MEIC inventory, http://www.meicmodel.org/; Li et al., 2014; Liu et al., 2015) for year 2010 is used to represent anthropogenic emissions.

The modeling system is initialized and forced at the lateral boundaries every day by 6 hourly data from the NCEP GFS at 0.5-degree resolution. For chemical species, previous modeling result is used for initial conditions. MOZART-4 historic data are employed as the gaseous chemical lateral boundary, and real time forecast of dust from the WRF-Dust model is employed as dust lateral boundary every 6 hours. More detailed information can be found in Zhou et al. (2017) and by contacting Jianming Xu (metxujm@163.com) at the Shanghai Meteorological Service.

2.8. WRF-CMAQ

A regional air quality operational forecasting system was developed at Nanjing University, China, on the basis of the WRF-CMAQ model. The version adopted for the WRF and CMAQ models are V3.5 and V4.7.1, respectively. Two nested domains with horizontal resolutions of 36 km and 12 km are adopted for the forecasts. The outer domain covers the entire continental region of China as well as surrounding countries in East Asia. The inner domain mainly focuses on the densely populated area of eastern China. The number of grid points adopted for the WRF model are 170 × 130 and 202 × 226, respectively with 51 sigma layers in vertical (12 layers below 1.5 km AGL) between the surface and the model top at 50 hPa. The CMAQ model is applied to the same domains but with three grid cells removed at each lateral boundary of the WRF domains. 15 vertical layers are selected from the 51 WRF layers, including about 8 layers in the boundary layer and 7 layers in the free troposphere.

Anthropogenic emissions are supplied offline from the MIX inventory (Li et al., 2017). Terrestrial biogenic emissions are calculated offline using MEGAN v2.04 (Guenther et al., 2006). Sea salt emissions are incorporated into the AERO4 aerosol module, and calculated online in CMAQ. Wind-blown dust is derived online from the WRF-Dust model. Open biomass-burning emissions are not considered here. It should be noted that the anthropogenic emissions are not fixed in this system, but are automatically adjusted every week according to the system performances in the past week and a series of simple and empirical relationships between emissions and concentrations.

The system provides every day a forecast for the next 192 hours. The NCEP Global Forecast System (GFS)'s products at 00 UTC are used for the initial and boundary conditions of the WRF model with a resolution of 0.5-degree and with a 3-hour interval. For the CMAQ model, the boundary conditions are created using idea profiles, and the chemical initial

fields are initialized from the previous forecasting. In addition, hourly averaged observed concentrations of SO_2, NO_2, CO, O_3, PM2.5 and PM10 from 1415 national control air quality-monitoring sites are assimilated into the initial fields using an optimal interpolation method [Lorenc, 1981]. More information on the code can be obtained from Fei Jiang (jiangf@nju.edu.cn) at Nanjing University. Informatio on WRF-CMAQ is also available on the web site http://carbon.nju.edu.cn/cn/ and https://www.epa.gov/cmaq/cmaq-models-0.

2.9. WARMS-CMAQ

The Community Multiscale Air Quality (CMAQ) model is a 3-D Eulerian chemical transport model that explicitly simulates emissions, gas-phase, aqueous, and mixed-phase chemistry, advection and dispersion, aerosol thermodynamics and physics, and wet and dry deposition. A detailed description and an evaluation of the CMAQ model are available in the papers by Byun and Schere (2006), Foley et al. (2010), and Appel et al. (2017). Here the CMAQ version 5.0.2 is adopted and includes the 2005 Carbon Bond (CB05) chemical mechanism (Yarwood et al., 2005) to represent the gas-phase chemistry. The fifth-generation modal CMAQ aerosol model (aero5) is adopted to formulate the aerosol chemistry and dynamics (Carlton et al., 2010).

In this version, CMAQ is used in an off-line mode. It is forced by pre-calculated hourly meteorological fields for the dynamics and by several emissions fluxes for the chemistry. Meteorology fields that drive chemical transport are produced by the Shanghai Meteorological Service (SMS) WRF ADAS Real-time Modeling System (WARMS). The SMS-WARMS has been extensively evaluated and is providing weather predictions in Eastern China. The modelling domain consists of 760 by 600 horizontal grids at 9-km resolution, with 51 layers in the vertical. As a subdomain of the SMS-WARMS run, the CMAQ domain consists of 430 by 370 horizontal grid cells at 9-km resolution. In the vertical, 26 layers are applied.

The anthropogenic emissions are based on monthly HTAP v2 dataset (http://edgar.jrc.ec.europa.eu/htap_v2/) (Janssens-Maenhout et al., 2015) for year 2010. As suggested by operational forecasting results, the HTAP NOx, SO_2 emissions are adjusted to account for rapid economic growth in the region. Biogenic emissions are estimated by the MEGAN model version 2.10 (Guenther et al., 2012). Currently, dust and biomass burning emissions are not included.

For the SMS-WARMS model forecasts, the NCEP GFS output at 0.5 degree is used as a background for ADAS data assimilation scheme, which ingests many local observations (e.g. radar and buoys), and to provide lateral boundary conditions. The chemical boundary conditions are currently based on the default vertical profiles of gaseous species and aerosols in CMAQ that represent clean air conditions. For more details, please contact Ying Xie (yxie33@outlook.com) at the Shanghai Meteorological Service. The CMAQ code is available on the US-EPA modeling site (https://github.com/USEPA/CMAQ/).

Geosci. Model Dev. Discuss., https://doi.org/10.5194/gmd-2018-144
Manuscript under review for journal Geosci. Model Dev.
Discussion started: 12 July 2018

Geoscientific Model Development Discussions

487 **Table 2a. Description of the Different Models**
488

Model and Institution	Model Documentation	Type of Model	Spatial Domain	Vertical and Horizontal Resolution	Meteo Data	Initial and Boundary Conditions
IFS ECMWF	CAMS	Global On-line	Global	60 vertical levels T511 (40 km)	ECMWF-IFS	IC: previous forecast corrected by data assimilation (analysis)
CHIMERE KNMI	Version 2013b	Regional Off-line	18-50^{0}N 102-132^{0}E	8 levels (surface to 500 hPa) 0.25 degree	ECMWF operational data	IC: previous forecast BC: LMDz-INCA (gas and particles), GOCART (mineral dust)
WRF-Chem-MPIM	Version 3.6	Regional On-line	Domain 1: 8S-51N 59-152E Domain 2: 18-45N 95-125E	51 levels (surf. to 10 hPa) Domain 1: 60 km x 60 km Domain 2: 20 km x 20 km	NCEP-FNL 6 hours 1^0 x 1^0	IC: previous forecast BC: IFS
SILAM FMI	Version 5.5	Regional Off-line	7-54N 67-147E	14 hybrid sigma-pressure levels up to ~ 400hPa 0.125^0 x 0.125^0	ECMWF-IFS	IC: previous forecast BC: Silam global forecast
EMEP MET Norway	Svn3064	Regional Off-line	15-55N 90-135E	20 sigma levels (surf. to 50 hPa)	ECMWF-IFS	IC: previous forecast BC: ECMWF IFS (3-hourly)
LOTOS-EUROS	Version 1.10	Regional Off-line	Domain 1: 15-50 N 71-139 E	5 layers (surf. to 5 km)	ECMWF-IFS	IC: previous forecast BC: CAMS

Geosci. Model Dev. Discuss., https://doi.org/10.5194/gmd-2018-144
Manuscript under review for journal Geosci. Model Dev.
Discussion started: 12 July 2018

			Domain 2: 20-45N 105-130^{E}	Domain 1: 0.5^{0} x 0.25^{0} Domain 2: 0.25^{0} x 0.125^{0}		C-IFS (3-hourly)
WRF-Chem SMS	Version 3.2	Regional On-line	20-44N 110-126E	28 vertical layers (surf. to 50 hPa) 6 km	NCEP GFS 6 hours 0.5^{0} x 0.5^{0}	IC: Previous run BC: MOZART monthly averages for 2009
WRF-CMAQ NJU	WRFv3.5 CMAQv 4.7.1	Regional Off-line	Domain 1: 18-52N, 78-136E Domain 2: 21-44N, 102-125E	Domain 1: 36 km x 36 km Domain 2: 12 km x 12 km WRF: 51 sigma levels CMAQ: 15 sigma levels	NCEP GFS 3 hours 0.5^{0} x 0.5^{0}	IC: Previous run BC: CMAQ default vertical profile
WARMS-CMAQ SMS	Version 5.0.2	Regional Off-line	14-53 N 100-144 E	26 sigma levels (from surf. to 50 hPa) 9 km	NCEP GFS 6 hours 0.5^{0} x 0.5^{0}	IC: Previous run BC: CMAQ default vertical profile

Table 2b. Continued

Model and Institution	PBL	Land-Use	Deposition	Chemistry	Data Assimilation
IFS ECMWF	IFS PBL scheme	IFS-Land use	Dry: Resistance Wet: in-cloud and below cloud scavenging and evaporation	Gas: CB05 Aerosol: LMDz/MACC	yes (O_3,CO,NO_2, SO_2,HCHO)
CHIMERE KNMI	bulk Richardson number (Menut et al., 2013)	GlobCover LandCover verion 2.3, 2009	Dry: Resistance Wet: in-cloud and below cloud scavenging	gas: MELCHIOR2 aerosol: Schemes for nucleation, absorption(ISORROPIA), and	no

Geosci. Model Dev. Discuss., https://doi.org/10.5194/gmd-2018-144
Manuscript under review for journal Geosci. Model Dev.
Discussion started: 12 July 2018

				coagulation	
WRF-Chem-MPIM	YSU	MODIS	Dry: Resistance Wet: in-cloud scavenging	gas: MOZART4 aerosol: GOCART	no
SILAM FMI	Bulk-Rishardson number, modified to use 2t and U*.	Maps of roughness, LAI from C-IFS	Dry: Resistance for gases, Kouznetsov&Sofiev (2012) for particles Wet: Rainout and washout with air-water equilibria	gas: CBM-IV aerosol: DMAT/VBS	not used
EMEP MET Norway	Slightly modified bulk Richardson number, PBL height always between 100-3000 m	GLC2000	Dry: Resistance Wet: in-cloud and below cloud scavenging	MARS module for aerosols Gas: EmChem09	no
LOTOS-EUROS	Version 1.10	Regional Off-line	Domain 1: 15-50 N 71-139 E Domain 2: 20-45N 105-130^{E}	5 layers (surf. to 5 km) Domain 1: 0.5^{0} x 0.25^{0} Domain 2: 0.25^{0} x 0.125^{0}	ECMWF-IFS
WRF-Chem SMS	YSU	MODIS	Dry: Resistance Wet: in-cloud scavenging	gas:RADM2 aerosol: ISORROPIA/SORGAM	no
WRF-CMAQ NJU	YSU	USGS modified with MODIS urban cover data	Dry: Resistance Wet: in-cloud and below cloud scavenging	Gas: CB05 Aerosol: aero4	Yes (SO_2, NO_2, CO, O_3, PM2.5, PM10)
WARMS-CMAQ SMS	YSU	MODIS	Dry: Resistance Wet: in-cloud and below cloud scavenging	gas: CB05 aerosol: CMAQ aero5	no

3. Adopted Emissions

The choice of the adopted surface emissions for primary chemical species has a significant influence on the atmospheric concentrations calculated for these species and for related secondary pollutants. In this inter-comparison exercise, the different groups involved have

Geosci. Model Dev. Discuss., https://doi.org/10.5194/gmd-2018-144
Manuscript under review for journal Geosci. Model Dev.
Discussion started: 12 July 2018

adopted their preferred anthropogenic emissions based on published inventories such as MEIC (Li et al., 2014; Liu et al., 2015), MACCity (Granier et al., 2011), EDGAR (Muntean et al., 2014; Crippa et al., 2016) and HTAP (Janssens-Maenhout et al., 2015). An inventory developed specifically for the PANDA project called PanHam has been obtained by combining information from the MEIC and HTAP inventories. Each model uses its own formulation for dust mobilization or seal salt emissions. In most cases, the biogenic emissions are derived online or offline from the MEGAN model (Guenther et al., 2006, 2012). Table 3 provides more details about the specified emissions and Figure 1 shows the mean distribution of the anthropogenic emissions for CO, NO and SO_2 adopted by different models during the period 1-14 March 2017. In the case of carbon monoxide, the adopted emissions are relatively similar in all models with mean emissions ranging from 4.0 to 4.6 mg m^{-2} h^{-1}. In the case of nitric oxide, however, there are substantial differences with mean emissions ranging from 0.31 mg m^{-2} h^{-1} (WRF-Chem-MPIM) to 0.99 mg m^{-2} h^{-1} (EMEP), but with values around 0.30 – 0.45 mg m^{-2} h^{-1} used by most models. For sulphur dioxide, produced primarily from coal combustion, the adopted values range from 0.31 mg m^{-2} h^{-1} (WRF-Chem-SMS) to 0.73 mg m^{-2} h^{-1} (IFS), but with values around 0.67 mg m^{-2} h^{-1} adopted in most models. The low values adopted for WRF-Chem-SMS reflect the likely impact of the recent measures taken in China to limit the emissions from coal burning facilities.

Emission inventories that are currently available to the modelling community usually account for anthropogenic emissions for years 2010 to 2012, and hence do not account for the substantial reduction in the emissions that took place since around 2014 as a result of actions taken by the Chinese authorities. The lower emission values adopted by several models may therefore be more realistic for providing chemical weather forecasts in 2017.

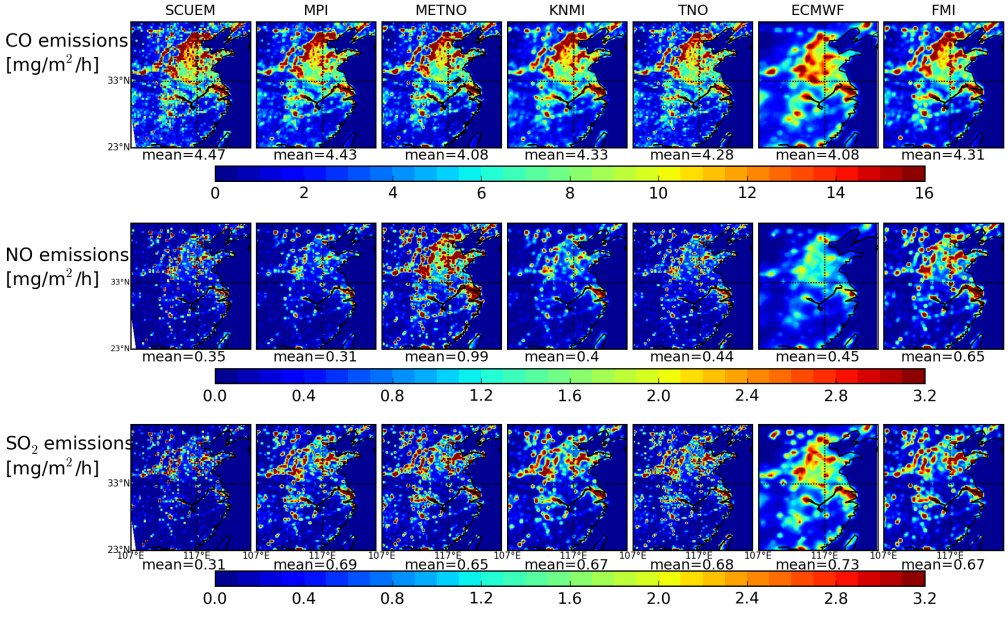

Geosci. Model Dev. Discuss., https://doi.org/10.5194/gmd-2018-144
Manuscript under review for journal Geosci. Model Dev.
Discussion started: 12 July 2018

528 **Figure 1.** Surface emissions of CO, NO and SO_2 [mg m^{-2} h^{-1}] adopted by the different models (average
529 for the period 1-14 March 2017). Note that the SCUEM emissions are those used in the WRF-Chem-
530 SMS model.
531
532
533
534 **Table 3. Adopted Emissions**
535

Model and Institution	Anthro. dataset	Dust	Seasalt	Biogenic	Biomass burning	Special Treatment/ Modification
IFS ECMWF	MACCity	Ginoux et al (2001)	Monahan et al. (1986)	Monthly climatology of MEGAN v2 run	GFAS	Diurnal cycle for isoprene
CHIMERE KNMI	MEIC 2010	none	none	MEGAN	none	none
WRF-Chem-MPIM	HTAPv2	GOCART	MOSAIC	MEGAN	none	Diurnal profiles by sector; Anthro NOx emission -50%;
SILAM FMI	MACCity with excluded Shippig, STEAM2015 Shipping, PanHam for Coarse PM	SILAM Scheme after Zender (2003)	SILAM Scheme Sofiev et al (2012)	MEGAN-MACC	GFAS (gases), IS4FIRES (PM)	Diurnal profiles by sector
EMEP MET Norway	PanHam (HTAP + MEIC2012)	none	Tsyro et al. (2011)	EMEP scheme	GFAS	none[1]
LOTOS-EUROS	EDGAR + MEIC2010	online	online	MEGAN	GFAS	Anthro NOx emission -35%; Anthro SO2 emission -50%
WRF-Chem SMS	MEIC 2010	With dust BC from WRF-Dust	none	MEGAN v2	none	Diurnal profiles by sector;

[1] Non during the inter-comparison exercise. Since summer 2017, however, the NOx emissions have been reduced by 35% in this particular model. The present version of the model also calculates windblown dust emissions from soil erosion.

Geosci. Model Dev. Discuss., https://doi.org/10.5194/gmd-2018-144
Manuscript under review for journal Geosci. Model Dev.
Discussion started: 12 July 2018

						Anthro NOx emission -40%; Anthro SO_2 emission -60%
WRF-CMAQ NJU	MIX	WRF-Dust	CMAQ scheme	MEGAN v2.04	none	Adjusted by performance of last week
WARMS-CMAQ SMS	HTAPv2	none	CMAQ scheme	MEGAN v2.10	none	Diurnal profiles by sector; Anthro NOx emission -50%; Anthro SO_2 emission -70%

4. Operational Forecasts provided by the MarcoPolo-Panda System.

As stated above, the MarcoPolo-Panda system is used operationally to provide daily forecast of air quality in eastern China. In its present configuration (Figure 2), the system is based on 9 models, which are executed independently on the computing system available in each respective partner institution. The outputs of the models are locally processed and the surface concentrations of the key chemical species are forwarded to a central database operated by the Royal Netherlands Meteorological Institute (KNMI). Ensemble mean and median concentrations are derived and, in addition to the forecasts from individual models, are posted on a dedicated website (www.marcopolo-panda.eu) and Chinese mirror site (http://116.62.195.108/). For the 37 Chinese cities with a population above 3 million in 2010, the predicted concentration values of ozone, NO_2, PM2.5 and PM10 are compared each hour to local measurements reported by the Chinese monitoring network (www.pm25.int). Observations for each city represent the mean of several measurements performed within one city (usually 5-12 stations). The data are averaged to city-centre coordinates.

We start by presenting a few examples of randomly selected forecasts as provided by the MarcoPolo-Panda system to illustrate the diversity among the models and the differences obtained under different situations. The performance of each individual model varies from day to day because it strongly depends on the individual weather forecast (meteorological situation, cloudiness, precipitation, etc.) that is adopted to simulate transport, photochemistry and deposition. Therefore this first description of model forecasts does not provide reliable information on the accuracy of the forecasts provided by the different models included in the ensemble.

Geosci. Model Dev. Discuss., https://doi.org/10.5194/gmd-2018-144
Manuscript under review for journal Geosci. Model Dev.
Discussion started: 12 July 2018

Geoscientific Model Development Discussions

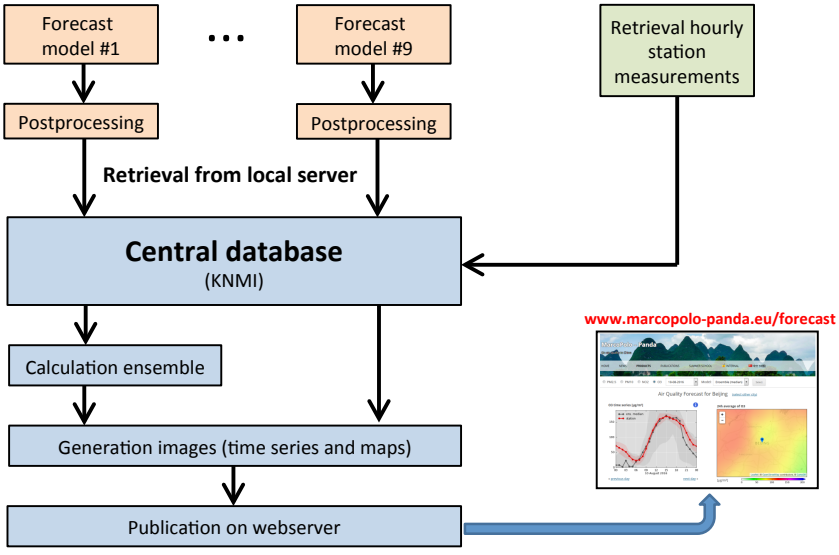

564
565
566 **Figure 2.** Structure of the operational multi-model forecast system with the 9 model components.
567 Postprocessed forecasts for the next 3 days provided by each model are sent to a central database
568 maintained by the Royal Netherlands Meteorological Institute (KNMI). Ensemble medians and
569 means are calculated and information (predicted daily variations of surface concentrations for 37
570 major Chinese cities, and maps of predicted diurnal mean surface concentrations) and are posted on
571 the http://www.marcopolo-panda.eu/forecast website. Users in China are redirected to the mirror
572 website maintained by SMS (http://116.62.195.108/). The forecasts are compared with the median
573 and mean observations provided by monitoring stations at different locations of the 37 cities.
574
575 The first example presents a relatively successful forecast made for the coastal city of
576 Xiamen in southeast China on 13 October 2017. The panels in Figure 3 show the excellent
577 agreement in the case of NO_2, ozone and PM2.5, suggesting that the median values derived
578 from the individual models capture well the features associated with the meteorological
579 situation, atmospheric transport and with the emissions in the region on that particular day.
580 The situation corresponds to very clean conditions with PM2.5 and NO_2 concentrations of
581 the order of 10 - 15 μg m^{-3}. The predicted ozone concentration ranges from 70 - 90 μg m^{-3}
582 (35 to 45 ppbv). Interestingly, however, the predicted PM10 concentrations are
583 underestimated during most of the day. The model predicts concentrations close to 20-25
584 μg m^{-3}, while the measurements indicate that the concentration reached values as high as
585 30-40 μg m^{-3}. The presence on October 13 of a strong wind flow in the strait between
586 Mainland China and Taiwan and associated with the Khanun tropical depression present on
587 this particular day west of the Philippines was likely a source of elevated sea salt emissions
588 and dust mobilization that may not have been properly captured by the models. Under such
589 strong meteorological disturbance, the forecast could be strongly resolution dependent.
590

Geosci. Model Dev. Discuss., https://doi.org/10.5194/gmd-2018-144
Manuscript under review for journal Geosci. Model Dev.
Discussion started: 12 July 2018

Geoscientific Model Development Discussions

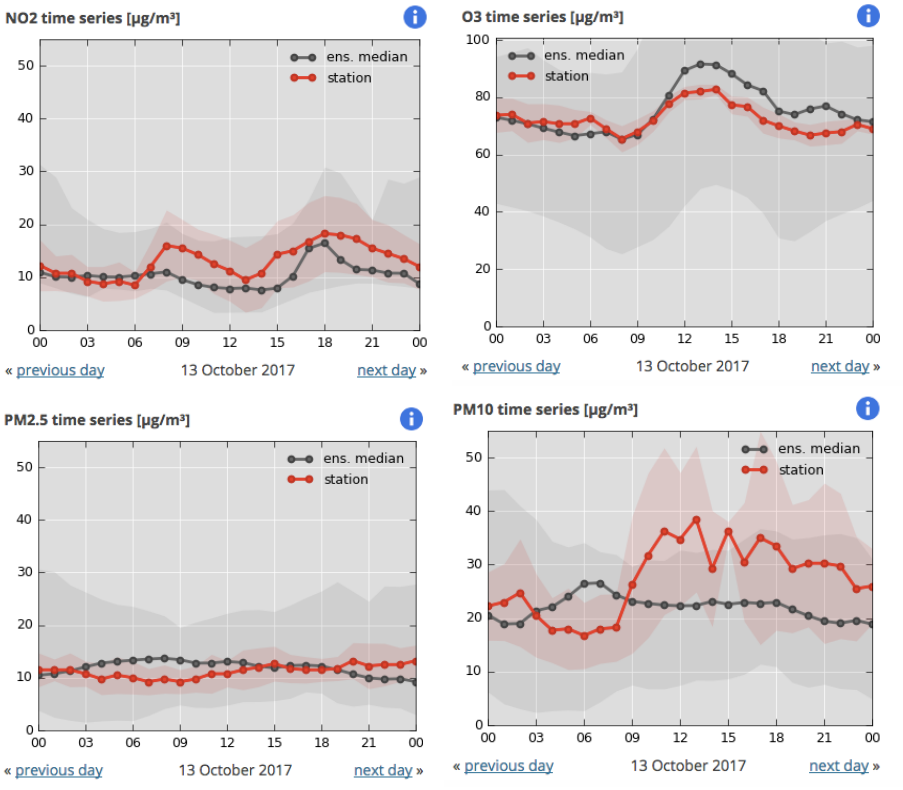

Figure 3. Median concentrations of NO_2 (upper, left), ozone (upper, right), PM2.5 (lower, left) and PM10 (lower, right) predicted for the city of Xiamen on 13 October, 2017 (black curve) and compared with the measured values (red curves). The dispersion of the forecasts by the individual models belong to the ensemble is shown by the grey range and the dispersion of the measured values at different stations in the city are depicted by the pink band.

The second example of predictions (Figure 4) refers to the forecast of $PM_{2.5}$ in Shanghai on a relatively polluted day (3 November, 2017). All models predict the presence of relatively high concentrations over land (diurnal mean values of typically 100 -150 µg m^{-3}) with a steep negative gradient towards the Chinese sea, where the concentrations are of the order of only 25-40 µg m^{-3}. Observations made at different stations in this urban area show the occurrence of two successive concentration peaks, one around 9:00-10:00 with concentrations reaching about 180 µg m^{-3} and the second one at 15:00-16:00 with concentrations as high as 150 µg m^{-3}. The ensemble mean forecast system predicts the occurrence of a single peak at about 7:00 am with a $PM_{2.5}$ concentration of about 220 µg m^{-3}. The forecast shows a gradual decrease in the concentration during the afternoon that is in good agreement with the observation. The occurrence of the second peak in the afternoon, however, is missed by the ensemble prediction, even though a peak appears in some of the individual model calculations (WRF-Chem SMS, EMEP and WRF-CMAQ), but often a few hours before it was actually detected by the monitoring stations. An inspection of the forecasts by the different models highlights the diversity in the model results. IFS, CHIMERE, WRF-Chem-SMS, and EMEP overestimate the PM2.5 concentrations before mid-day, while

Geosci. Model Dev. Discuss., https://doi.org/10.5194/gmd-2018-144
Manuscript under review for journal Geosci. Model Dev.
Discussion started: 12 July 2018

they provide values in good agreement with the observations in the afternoon and evening. WRF-Chem-MPIM underestimates the concentrations during the entire day. LOTOS-EUROS as well as WRF-CMAQ provide values that are in fair agreement with the observations in the morning, but underestimate the concentrations in the afternoon.

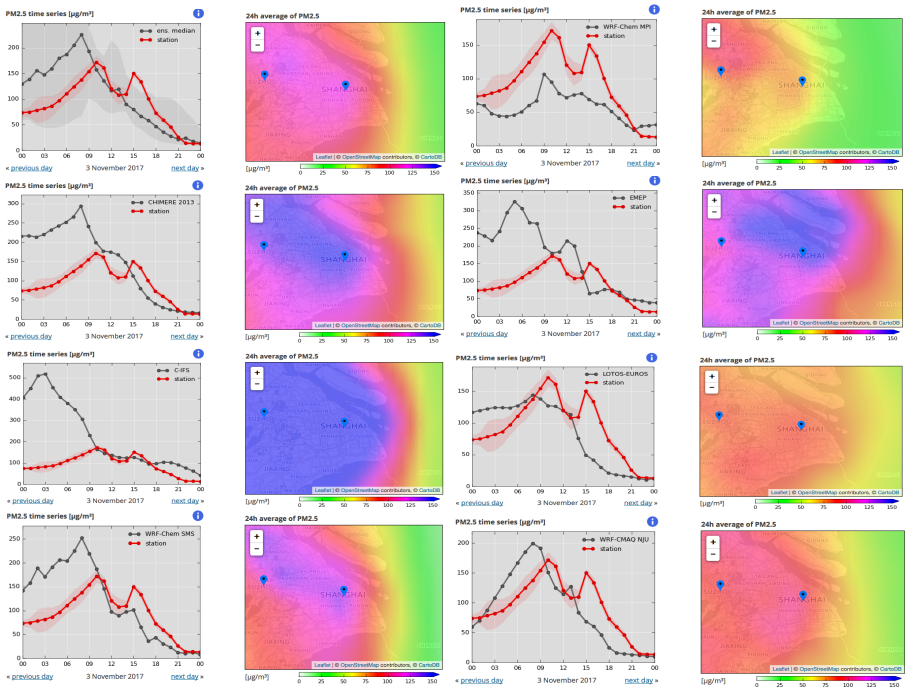

Figure 4. Forecast by different models of $PM_{2.5}$ concentration during a polluted day in Shanghai on 3 November 2017. The graph at the top left represents the median concentration, and the individual forecasts provided by CHIMERE, IFS, WRF-Chem-SMS, WRF-Chem-MPIM, EMEP, LOTOS-EUROS, and WRF-CMAQ are shown by the other panels.

A third example (Figure 5) refers to the predicted concentration of $PM_{2.5}$ on 25 October 2017 in Beijing. In this particular case, the ensemble forecast system predicts the occurrence of a rather polluted day with stagnant air and high concentrations of aerosol particles over Beijing as a band stretching from the southwest to the northeast. The median concentration predicted for this day is close to 200 µg m^{-3}, but is a factor 2 higher than the observation. Most individual models produce this band of high PM2.5 concentrations with the exception of the WRF-Chem-MPIM model that shows moderate levels of pollution with an aerosol cloud localized in the urban area of Beijing. An examination of the results provided by the individual models shows again large differences. Some models (CHIMERE, EMEP, LOTOS-EUROS, WRF-Chem-MPIM) calculate a slow and rather steady concentration increase during the day, while other models (WRF-Chem-SMS, WARMS-CMAQ-SMS, SILAM and IFS) exhibit some irregular variations during the day. Most models overestimate the $PM_{2.5}$ concentrations except LOTOS-EUROS and WRF-Chem-MPIM, which predict

Geosci. Model Dev. Discuss., https://doi.org/10.5194/gmd-2018-144
Manuscript under review for journal Geosci. Model Dev.
Discussion started: 12 July 2018

644 concentrations with the same order of magnitude as the observations at the monitoring
645 stations.

Geosci. Model Dev. Discuss., https://doi.org/10.5194/gmd-2018-144
Manuscript under review for journal Geosci. Model Dev.
Discussion started: 12 July 2018

Geoscientific Model Development Discussions

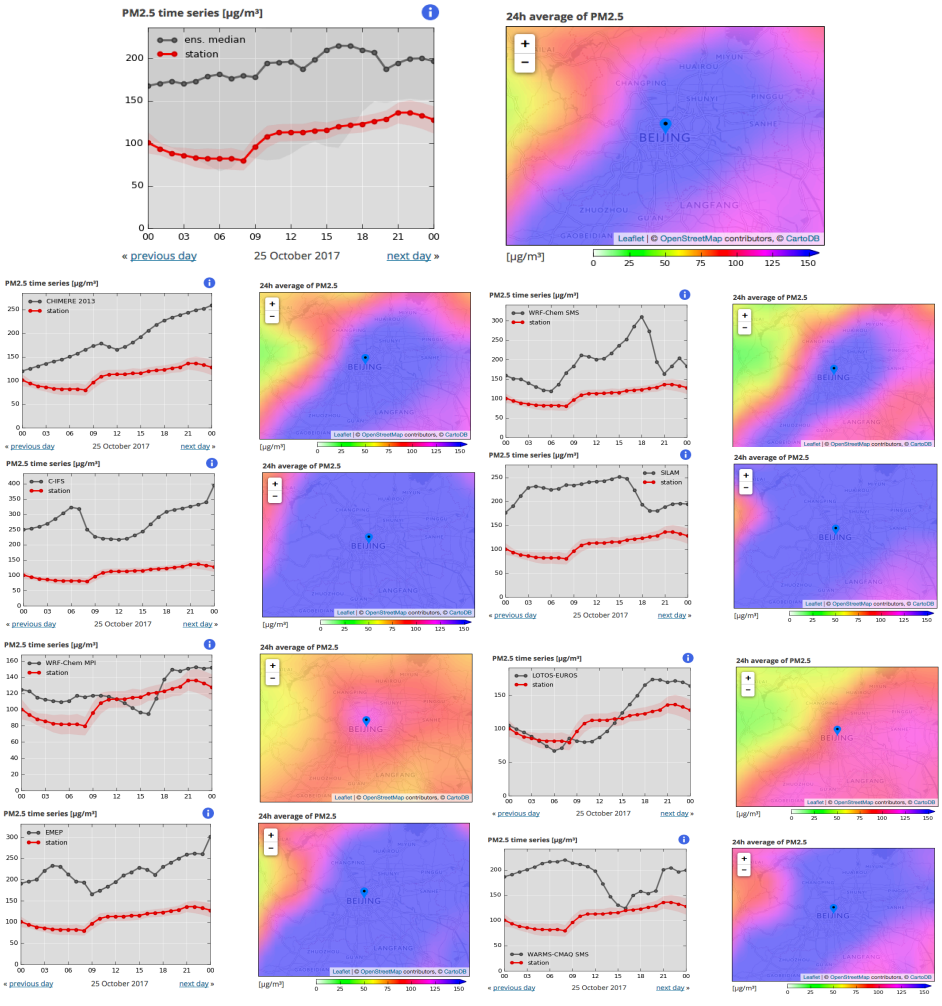

Figure 5. Diversity of $PM_{2.5}$ forecasts in Beijing on 25 October 2017 by several models included in the ensemble of the MarcoPolo-Panda prediction system. The ensemble median is shown by the top panels, and the individual forecasts provided by CHIMERE, IFS, WRF-Chem-MPIM, EMEP, WRF-Chem-SMS, SILAM, LOTOS-EUROS, and WARMS-CMAQ-SMS are shown by the other panels.

The last illustrative example refers to the forecast of nitrogen oxides and ozone in the Shanghai area on 31 October 2017 (Figure 6a, b and c). All models show that the NO_2 concentrations are highest in the boundary layer of the urban areas, even though the calculated values may be different from model to model, and the dispersion of the species away from the urban centres may also be uneven. In all cases, predicted values above the ocean are very low, i.e., less than a few µg m^{-3}. A band of high NO_2 concentrations extends from Shanghai in the northwest direction.

The median values of NO_2 in the city (top panels) are in good agreement with the observed values, with night-time concentrations on the order of 60-80 µg m^{-3}, and substantially lower values during daytime resulting from the photolysis of the molecule by solar radiation. A minimum concentration of 25 µg m^{-3} is reached around noon.

The diurnal variation of NO_2 is well captured by most models, in particular by CHIMERE (although the absolute values are too low), IFS, WRF-Chem-SMS, WRF-Chem-MPIM and WARMS-CMAQ-SMS. The diurnal variation is somewhat underestimated in EMEP, LOTOS-EUROS and WRF-CMAQ.

The ozone concentration (right panels) also exhibits a strong diurnal variation that, to a large extent, mirrors the NO_2 variation. Measurements show a maximum value of nearly 100 µg m^{-3} reached at 15:00 and low night-time concentrations (typically 10-30 µg m^{-3}). The median concentrations, provided by the ensemble forecast system upper panel on the right), are characterized by a similar diurnal variation but with lower amplitude. The concentration reaches its maximum at 14:00, but the value of this maximum is only equal to 60 µg m^{-3}. The values predicted for the night are generally somewhat smaller than the observation, with values of the order of 5-10 µg m^{-3}.

In the case of ozone, differences between model forecasts are again substantial. The maximum concentration values in the early afternoon are 50 µg m^{-3} for CHIMERE, 62 µg m^{-3} for IFS, 85 µg m^{-3} for WRF-Chem-SMS, 65 µg m^{-3} for WRF-Chem-MPIM, 30 µg m^{-3} for EMEP, 42 µg m^{-3} for LOTOS-EUROS, 57 µg m^{-3} for WRF-CMAQ and 100 µg m^{-3} for WARMS-CMAQ-SMS.

Geosci. Model Dev. Discuss., https://doi.org/10.5194/gmd-2018-144
Manuscript under review for journal Geosci. Model Dev.
Discussion started: 12 July 2018

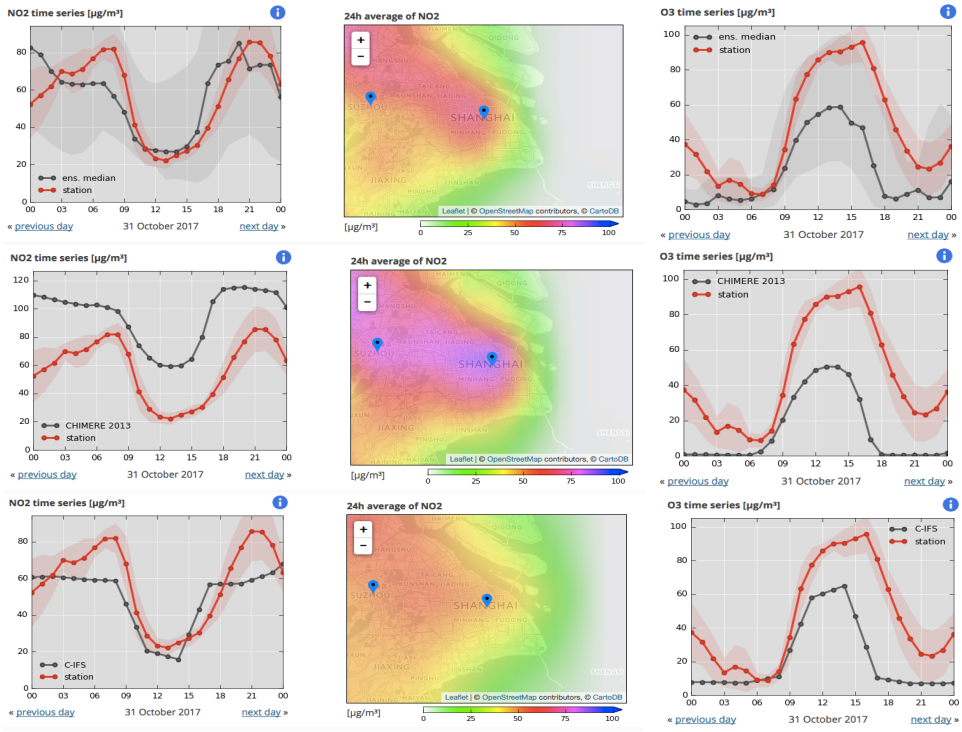

Figure 6a. Diversity in the NO_2 and ozone forecasts made for Shanghai on 31 October 2017 as highlighted by the predictions from several models included in the ensemble of the MarcoPolo-Panda system. The left and right panels show the diurnal variation of the predicted (black) and observed (red) NO_2 and ozone concentrations (µg m^{-3}), respectively. The center panel presents the geographical distribution in the vicinity of Shanghai of the diurnal average predicted for the NO_2 concentration. The ensemble median is shown in the top panels, and two individual forecasts as provided by CHIMERE and IFS are shown in the middle and lower panels.

Geosci. Model Dev. Discuss., https://doi.org/10.5194/gmd-2018-144
Manuscript under review for journal Geosci. Model Dev.
Discussion started: 12 July 2018

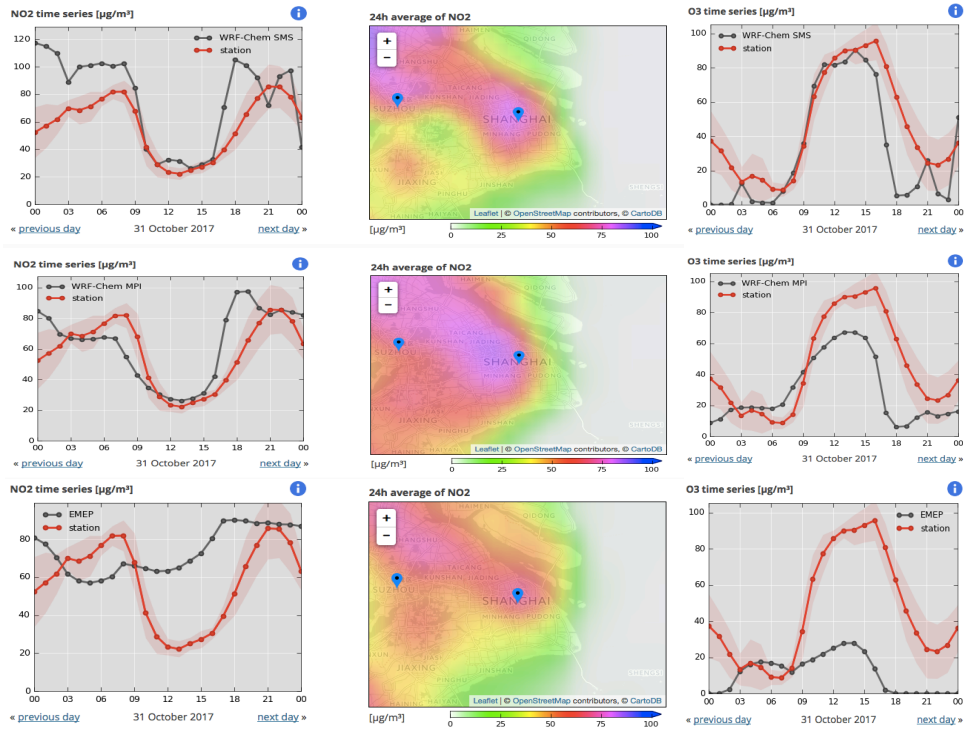

Figure 6b. Same as in Figure 6a, but for the individual forecasts from WRF-Chem-SMS, WRF-Chem-MPIM and EMEP.

Geosci. Model Dev. Discuss., https://doi.org/10.5194/gmd-2018-144
Manuscript under review for journal Geosci. Model Dev.
Discussion started: 12 July 2018

Geoscientific Model Development Discussions

706

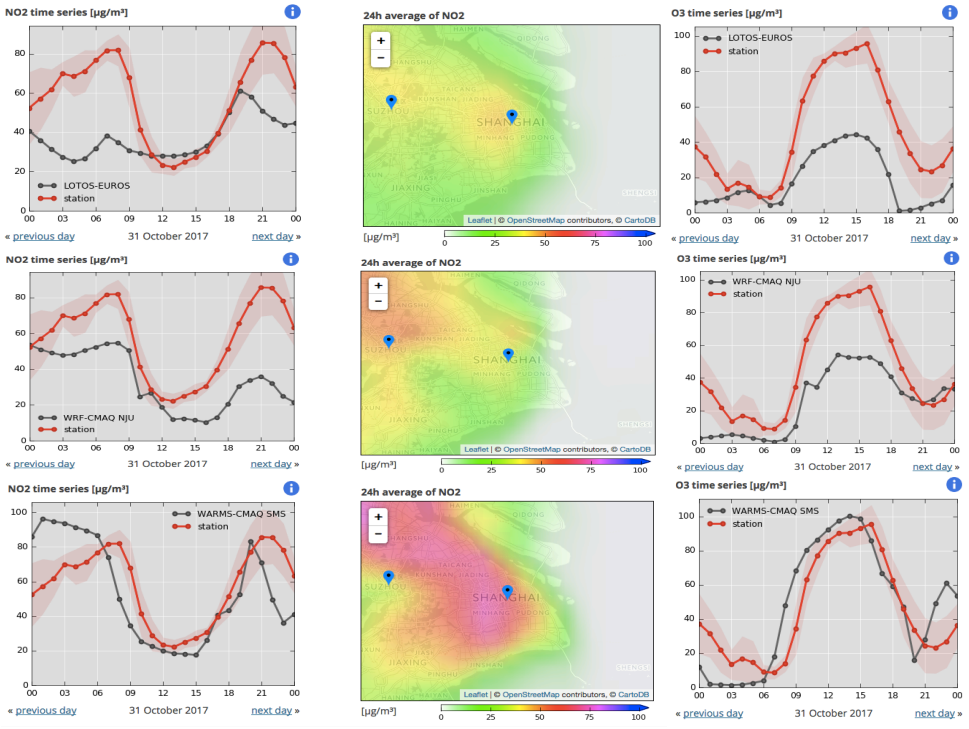

707
708
709 **Figure 6c.** Same as Figure 6a but for the individual forecasts from LOTOS-EUROS, WRF-CMAQ and
710 WARMS-CMAQ.
711
712
713

Geosci. Model Dev. Discuss., https://doi.org/10.5194/gmd-2018-144
Manuscript under review for journal Geosci. Model Dev.
Discussion started: 12 July 2018

5. Inter-comparison of Individual Models

We now present an inter-comparison of most of the models included in the operational MarcoPolo-Panda System. The participants to this inter-comparison examined in detail the daily forecasts performed for the month of March 2017 with particular emphasis on the results obtained during the first two weeks of the month.

In the following Sections, we present selected chemical fields derived by the different models that participated in the comparison exercise, and highlight similarities and differences with the purpose of identifying the causes of the discrepancies between models and between models and observations. We first examine monthly mean surface concentrations obtained from a subset of the models involved in the inter-comparison. We then compare the time evolution associated with the model forecasts with observations made at specific surface measurement sites and present some correlations between calculated and measured concentrations at these sites.

5.1. Comparison of average fields

We first compare the March 2017 monthly mean concentrations of different chemical species calculated by 7 models (IFS, LOTOS-EUROS, EMEP, SILAM, WRF-Chem-MPIM, WRF-Chem-SMS and CHIMERE) with surface measurements reported at different sites in the eastern part of China (www.pm25.int). Figure 7a shows the calculated and observed surface concentrations of carbon monoxide (CO). We first note the substantial differences that exist between the individual model forecasts, probably reflecting differences in the adopted emissions or in the atmospheric production resulting from the oxidation of volatile organic compounds in the planetary boundary layer. Observations indicate that CO concentrations are generally higher than 900 ppbv, except near the south-eastern coast and in the south-western part of the country, where the values are as low as 500 to 700 ppbv. The models show considerably lower values, ranging from about 300-500 ppbv. The regions with the highest mean concentrations are located in the North China Plain (NCP), where values higher than 1200 ppbv are recorded. Relatively high values (close to 1000 ppbv) are also found in some urban areas (e.g., Hong Kong) near the south coast of the country.

The models provide a rather different picture: most of them substantially underestimate the CO concentrations, in particular WRF-Chem-SMS, WRF-Chem-MPIM, EMEP and LOTOS EUROS. Higher concentrations are derived by SILAM and IFS. These models, however, produce peak concentrations in the region of Sichuan Basin in contrast with the observations. Only IFS reproduces the high concentrations observed in northern China. Clearly, the performance of the models regarding the calculation of CO concentrations is not satisfactory. The discrepancies may be attributed to an underestimation of CO emissions, errors in the lateral boundary conditions or indirectly to an underestimation of the emissions for primary hydrocarbons.

Geosci. Model Dev. Discuss., https://doi.org/10.5194/gmd-2018-144
Manuscript under review for journal Geosci. Model Dev.
Discussion started: 12 July 2018

We first compare the March 2017 monthly mean concentrations of different chemical species calculated by 7 models (IFS, LOTOS-EUROS, EMEP, SILAM, WRF-Chem-MPIM, WRF-Chem-SMS and CHIMERE) with surface measurements reported at different sites in the eastern part of China. Figure 7a shows the calculated and observed surface concentrations of carbon monoxide (CO). We first note the substantial differences that exist between the individual model forecasts, probably reflecting differences in the atmospheric production of CO resulting from the oxidation of volatile organic compounds or from the chemical destruction of CO occurring in the planetary boundary layer. Observations indicate that CO concentrations are generally higher than 900 ppbv, except near the south-eastern coast and in the south-western part of the country, where the values are as low as 500 to 700 ppbv. The regions with the highest mean observed concentrations are located in the North China Plain (NCP), where values higher than 1200 ppbv are recorded. Relatively high values (close to 1000 ppbv) are also found in some urban areas (e.g., Hong Kong) near the south coast of the country.

The models provide a rather different picture: most of them substantially underestimate the CO concentrations, in particular WRF-Chem-SMS, WRF-Chem-MPIM, EMEP and LOTOS EUROS with calculated values ranging from about 300-500 ppbv. Higher concentrations are derived by SILAM and IFS. These models, however, produce peak concentrations in the region of Sichuan Basin in contrast with the observations. Only IFS reproduces the high concentrations observed in northern China. Clearly, the performance of the models regarding the calculation of CO concentrations is not satisfactory. The discrepancies may be attributed to an underestimation of CO emissions, errors in injection height or overestimation of mixing/boundary layer height, errors in the lateral boundary conditions or indirectly an underestimation of the emissions for the primary hydrocarbons.

Geosci. Model Dev. Discuss., https://doi.org/10.5194/gmd-2018-144
Manuscript under review for journal Geosci. Model Dev.
Discussion started: 12 July 2018

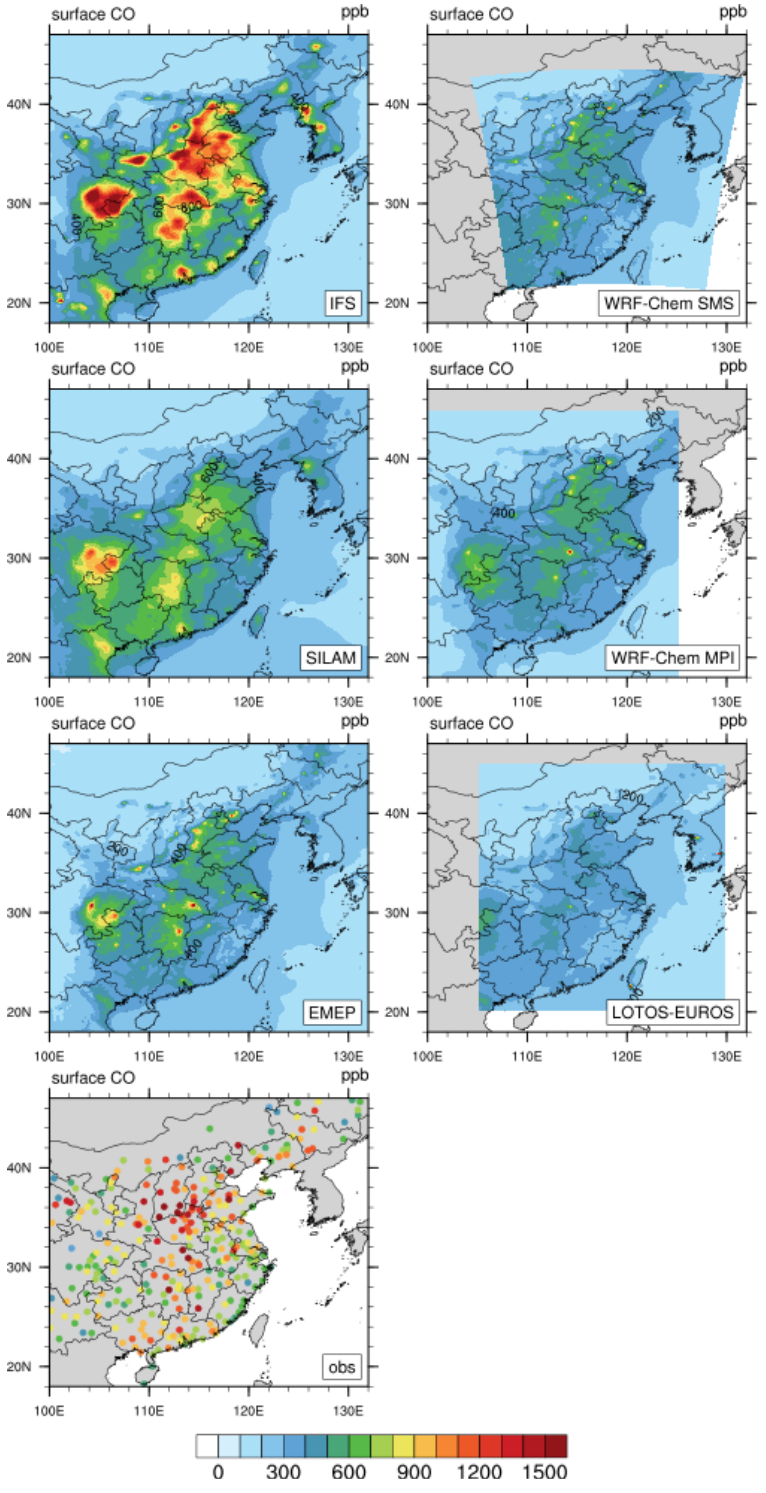

788

Geosci. Model Dev. Discuss., https://doi.org/10.5194/gmd-2018-144
Manuscript under review for journal Geosci. Model Dev.
Discussion started: 12 July 2018

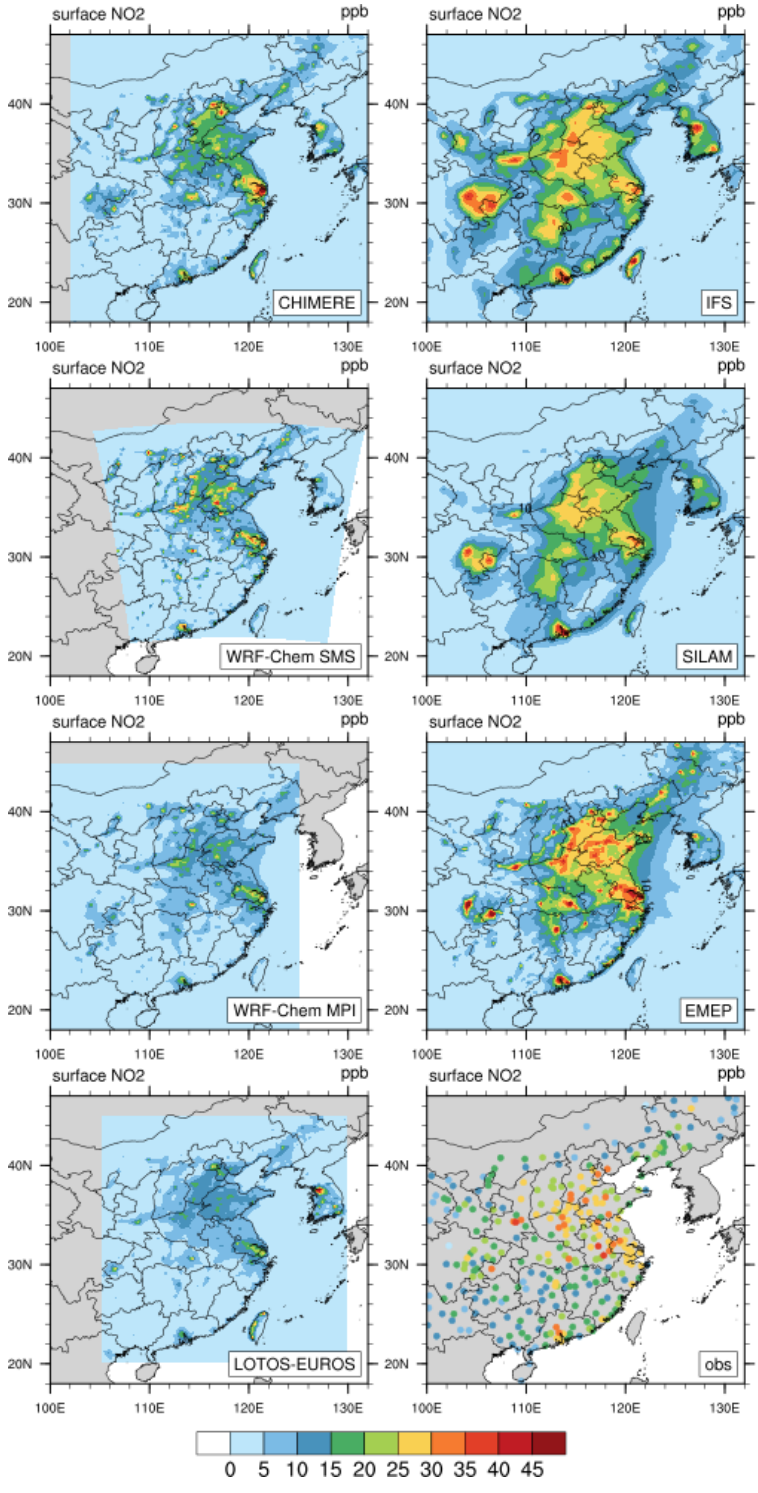

Geosci. Model Dev. Discuss., https://doi.org/10.5194/gmd-2018-144
Manuscript under review for journal Geosci. Model Dev.
Discussion started: 12 July 2018

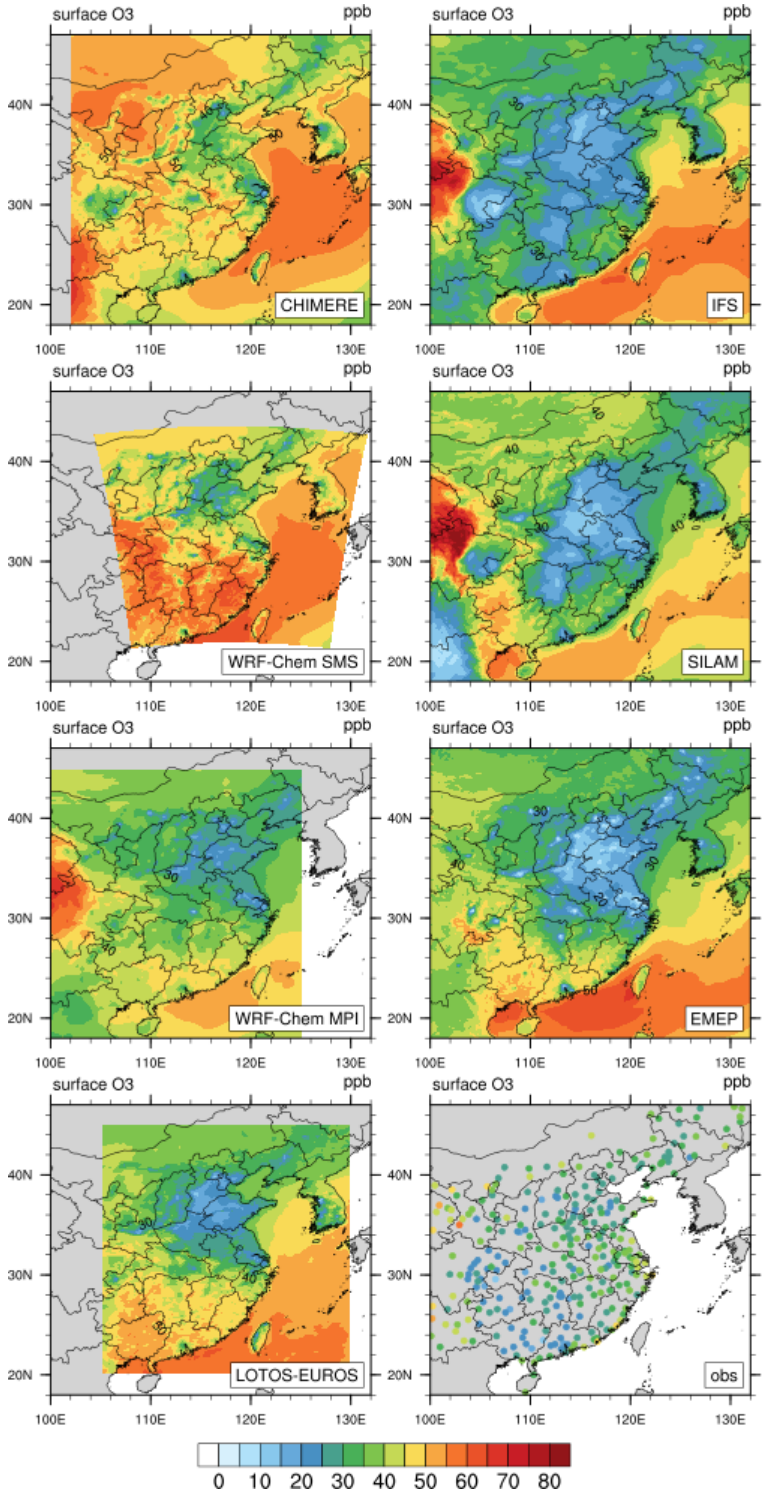

790

Geosci. Model Dev. Discuss., https://doi.org/10.5194/gmd-2018-144
Manuscript under review for journal Geosci. Model Dev.
Discussion started: 12 July 2018

791

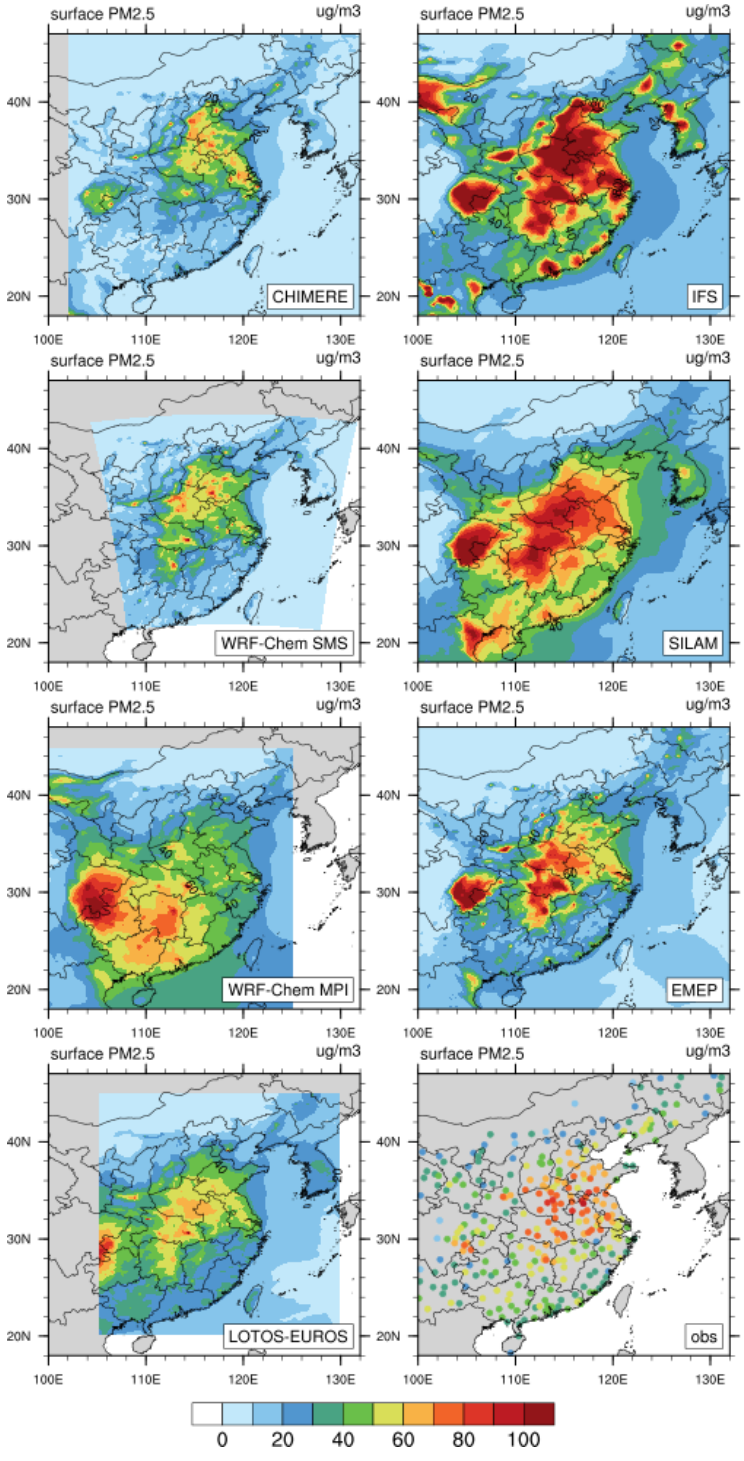

792

Figure 7. Monthly mean surface concentrations of CO, NO_2, ozone (ppbv), and PM2.5 (μg m^{-3}) provided for the month of March 2017 by different models: CHIMERE (no CO), IFS, WRF-Chem-SMS, SILAM, WRF-Chem-MPIM, EMEP and LOTOS-EUROS. The monthly mean concentration values derived from observations at different monitoring stations are represented by dots in one of the lowest panels. The adopted colour scales are the same as the colour scales adopted to represent the model results.

In the case of NO_2 (Figure 7b), the observations show that the surface concentrations are highest in the north-eastern portion of China with a few urban hotspots. These patterns are well reproduced by the EMEP, SILAM and IFS models. The other models also produce high concentrations in urban areas, but with values that are lower than those provided by the monitoring stations.

The mean surface ozone concentrations derived from measurements are lowest (about 20 ppbv) in the central part of China and highest (30-40 ppbv) near the east coast (Shanghai region), the south coast and the western part of China. Since nitrogen oxides tend to titrate ozone, the models that predict high NO_2 concentrations derive the lowest ozone values (EMEP, SILAM, IFS). The high NO_2 concentrations predicted by EMEP are probably related to the large emissions used as shown in Fig 1. CHIMERE, WRF-Chem-SMS and to a lesser extent WRF-Chem-MPIM overestimate the mean ozone concentration during March. All models, however, produce a minimum in the ozone concentrations in north-eastern China, a pattern that is not visible in the observational data (Figure 7c).

Finally, in the case of PM2.5 (Figure 7d), the measurements suggest the presence of high concentrations (higher than 80 μg m^{-3}) in the region between Beijing and Shanghai. High abundances of PM2.5 are derived in this region by IFS, SILAM and to a lesser extent by LOTOS-EUROS, EMEP, CHIMERE and WRF-Chem-SMS. Interestingly, most models produce another marked hotspot in the region of Sichuan Basin, while the observations suggest a less pronounced maximum with a more limited geographical extent.

5.2. Time Evolution of Median Forecasts

We now focus on the time period during which the most intensive comparison between models has been performed. We first examine the time evolution of surface ozone, NO_2 and $PM_{2.5}$ produced by the different models for the time period ranging from 1 to 15 March 2017, and for the three large metropolitan areas: Beijing, Shanghai and Guangzhou. In Figure 8, we compare the median concentrations of the three species with the median values derived from the different measurements provided by the network of instruments deployed in the three cities. The median model values are represented by the red curves, while the shaded areas highlight the dispersion of the calculated concentrations around the median values.

Beijing. Here the predictions of the $PM_{2.5}$ concentrations follow very closely the observations. Two events with relatively high aerosol loads are visible, the first one between 2 and 5 March and the second one on 11 March. In the case of NO_2, the models reproduce

Geosci. Model Dev. Discuss., https://doi.org/10.5194/gmd-2018-144
Manuscript under review for journal Geosci. Model Dev.
Discussion started: 12 July 2018

841 fairly well the daily variability reported by the monitoring stations, but on the average they
842 slightly underestimate the concentrations values. The high concentrations appearing
843 between 2 and 5 March and between 10 and 11 March are well captured by the median of
844 the models. Finally, the models reproduce the diurnal variability in the ozone
845 concentrations, but they overestimate these concentrations by typically 20 μg m^{-3}.
846
847 *Shanghai*. The calculated median concentrations of $PM_{2.5}$ are in good agreement with the
848 observations, especially between 10 and 15 March. During the first part of the simulation,
849 the mean measured and calculated values are close, but the models fail to capture high
850 peaks such as those observed on 3, 6, 8 and 9 March. In the case of NO_2, the agreement
851 between calculated and measured concentrations is good. Again, the models severely
852 overestimate the ozone concentrations.
853
854 *Guangzhou.* The median concentration of $PM_{2.5}$ provided by the model is similar to the
855 observation between 1 and 7 March. However, the model underestimates the
856 concentrations between 7 and 11 March and overestimates them between 12 and 14
857 March. For NO_2, the agreement between models and measurements is relatively good
858 during the first days of the month, but the models fail to reproduce the substantial daily
859 variability observed after 6 March. Ozone is well simulated in this particular urban area,
860 even though the daily peaks are sometimes over- or underestimated.
861

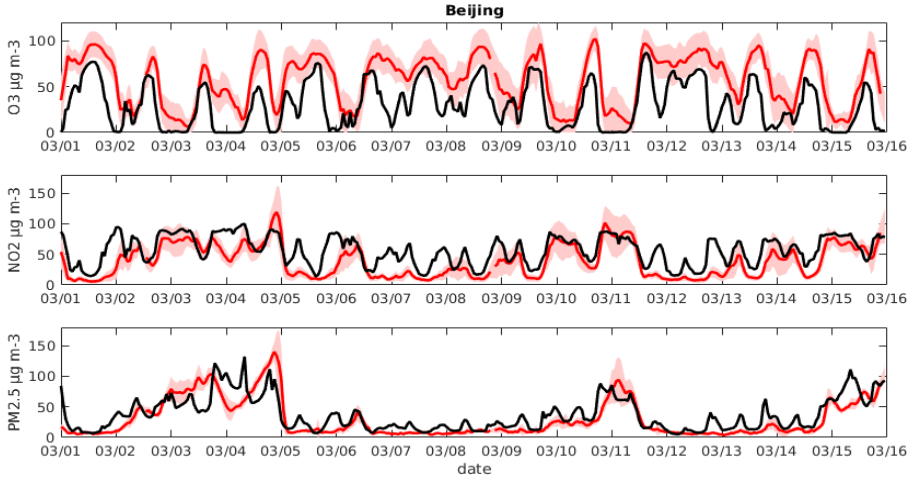

862

Geosci. Model Dev. Discuss., https://doi.org/10.5194/gmd-2018-144
Manuscript under review for journal Geosci. Model Dev.
Discussion started: 12 July 2018

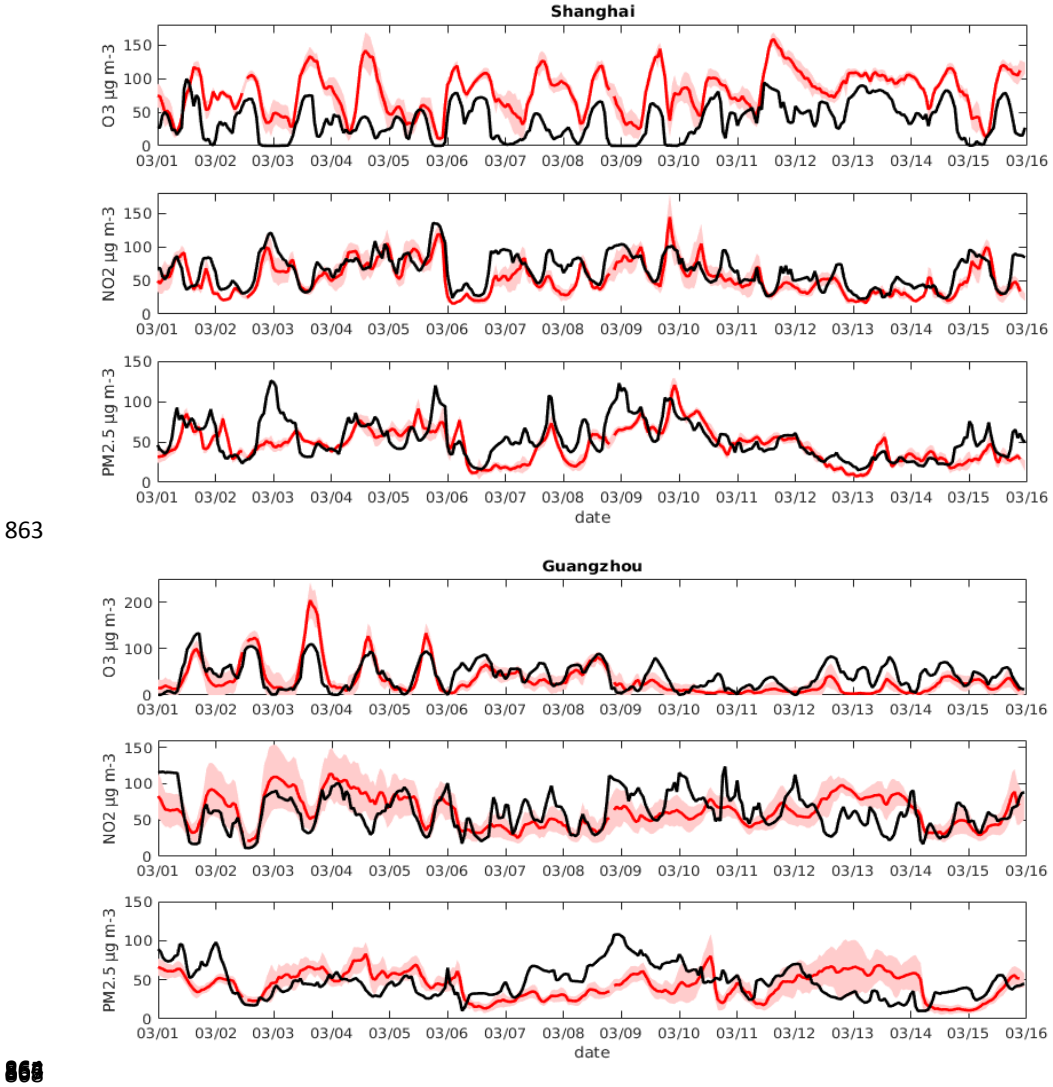

Figure 8. Evolution of the surface concentrations of ozone, nitrogen dioxide and particulate matter (diameter less than 2.5 microns). In red: median of calculated values by the different models, and in black: observed median concentrations.

5.3. Statistical Errors

In order to measure the performance of the individual models involved in the present inter-comparison, we have calculated statistical measures of the model results for the chosen period of 1-15 March 2017. These measures include the mean bias (BIAS), the mean normalized bias (MNMBIAS), the root mean square error (RMSE), the fractional gross error (FGE) and the correlation coefficient for ozone, NO_2 and PM2.5 (Table 4). They apply to the

Geosci. Model Dev. Discuss., https://doi.org/10.5194/gmd-2018-144
Manuscript under review for journal Geosci. Model Dev.
Discussion started: 12 July 2018

data for the 37 cities considered in the MarcoPolo-Panda forecast system. The same statistical measures are also provided for the ensemble median.

Table 4: For the period 1st to 15th March 2017, statistical measures (mean bias (BIAS), mean normalized bias (MNB), root mean square error (RMSE), FGE (fractional gross error) and correlation coefficient calculated for the forecast of O_3, NO_2 and $PM_{2.5}$ concentrations for all models and for the ensemble median at all stations/cities, for which the MarcoPolo-Panda Forecast is available. The correlation is based on 1-hourly data.

		Ensemble Median	CHIMERE	IFS	WRF-Chem SMS	SILAM	WRF-Chem MPIM	EMEP	LOTOS-EUROS
BIAS ($\mu g\ m^{-3}$)	O3	-14.7	-5.9	-13.1	13.2	-25.8	-23.9	-23.3	-4.0
	NO2	-3.0	-4.8	-2.0	-4.2	-3.1	8.4	11.2	-20.7
	PM2.5	3.7	-2.0	39.7	-4.5	21.7	5.5	12.4	-4.7
MNB (%)	O3	-41%	-24%	-51%	13%	-74%	-69%	-74%	-7%
	NO2	-8%	-18%	-13%	-19%	-11%	13%	15%	-52%
	PM2.5	8%	-4%	44%	-18%	22%	11%	9%	-7%
RMSE ($\mu g\ m^{-3}$)	O3	32.8	27.0	29.4	41.8	44.6	44.7	42.9	37.2
	NO2	21.8	24.4	23.1	31.9	28.5	28.9	34.0	34.4
	PM2.5	30.2	31.5	71.3	35.8	47.7	39.1	52.4	27.3
FGE (%)	O3	70%	58%	72%	64%	99%	97%	99%	65%
	NO2	38%	45%	44%	53%	51%	43%	48%	66%
	PM2.5	38%	44%	62%	54%	52%	49%	47%	39%
Corr. Coeff.	O3	0.60	0.70	0.72	0.45	0.32	0.32	0.39	0.38
	NO2	0.64	0.62	0.65	0.47	0.41	0.50	0.46	0.31
	PM2.5	0.62	0.55	0.47	0.54	0.66	0.36	0.49	0.64

When examining the mean bias of the ensemble median, the values are equal to -14.7, -3.0 and +3.7 $\mu g\ m^{-3}$ for ozone, NO_2 and PM2.5, respectively, to be compared to mean concentration values of the order of 50 $\mu g\ m^{-3}$ for these three different species. Table 4 shows in the case of ozone, individual models are characterized by biases ranging from -25.8 (SILAM) to +13.2 $\mu g\ m^{-3}$ (WRF-Chem-SMS) with the smallest absolute value equal to 5.9 $\mu g\ m^{-3}$ (CHIMERE) The corresponding numbers range from – 20.7 $\mu g\ m^{-3}$ (LOTOS-EUROS) to + 11.2 $\mu g\ m^{-3}$ (EMEP) with the smallest absolute bias of -2.0 $\mu g\ m^{-3}$ (IFS) for NO_2. For PM2.5, they range from -4.7 $\mu g\ m^{-3}$ (LOTOS-EUROS) to +39.6 $\mu g\ m^{-3}$ (IFS) with the smallest absolute value equal to -2.0 $\mu g\ m^{-3}$ (CHIMERE). In general, during the period chosen for the inter-comparison, the models underestimate the ozone and NO_2 concentrations and overestimate the concentration of PM2.5. The table also shows that the RMSE for the median values for ozone, NO_2 and PM2.5 are 32.8, 21.8 and 30.2 $\mu g\ m^{-3}$, respectively. With some exception (CHIMERE and IFS for ozone, LOTOS-EUROS for PM2.5), these values are

lower than the RMSE derived by individual models. The highest values for RSME are 44.7 μg m^{-3} (WRF-Chem-MPIM) in the case of ozone, 34.4 (LOTOS EUROS) in the case of NO_2, and 71.3 (IFS) in the case of PM2.5. The smallest RMSE are equal to 27.0 μg m^{-3} (CHIMERE) in the case of ozone, 23.1 μg m^{-3} (IFS) in the case of NO_2 and 27.3 μg m^{-3} in the case of PM2.5 (LOTOS-EUROS). The correlation coefficient for the ensemble median is of the order of 0.6 for the three species, which in most cases is higher than the values derived from individual model forecasts. There are few exceptions, however. The correlation coefficients are higher in the forecast of ozone by CHIMERE (0.70) and IFS (0.72), in the case of NO_2 by IFS (0.65) and in the case of PM2.5 by SILAM (0.66) and LOTOS-EUROS (0.64). Table 5 summarizes the models that have achieved the best performance from the point of view of the mean bias, the RMSE and the correlation coefficient.

.

Table 5. Best Model Performance

Statistical Variable	Best performance ozone	Best performance NO2	Best performance PM2.5
Mean Bias	LOTOS-EUROS	IFS	CHIMERE
RMSE	CHIMERE	IFS	LOTOS-EUROS
Correlation coefficient	IFS	WRF-Chem MPIM	SILAM

5.4. Time Evolution of Individual Forecasts

The time evolution of predicted concentration values at Beijing by 5 different models involved in the inter-comparison is provided in Figure 9 for the period of 1-15 March 2017. An examination of the figure shows that, during most days, the daytime height of the PBL reaches 2500 – 3000 m with an exception on 2 to 5 March, when the height does not exceed 1000 m. Interestingly, during this period, the observed concentration of particulates, of NO_2 and of SO_2, strongly influenced by surface emissions, are significantly higher than during the following days. During the same days, the night-time concentration of ozone is relatively low. On March 10, one also observes high surface concentrations of emitted species and low concentration of night-time ozone, even though the calculated PBL height is not particularly low. One should mention here that in several models (i.e., EMEP, LOTOS-EUROS) the information on the PBL is deduced from the IFS forecast, while in other models (such as WRF-Chem-MPIM and WRFChem-SMS) the PBL height is derived independently. In the case of WRF-Chem-MPI, however, the calculation makes of meteorological data taken from the IFS model.

In most cases, the models capture relatively well the day-to-day variability in the species concentrations. The agreement with observations is generally good in the case of PM2.5 and PM10, except in the case of the IFS model, which considerably overestimates the concentrations, mainly because of a regional overestimation of the OM emissions and a lack of a diurnal variation of the emission The anthropogenic OM emissions in IFS are parameterised based on anthropogenic CO emissions following Spracklen et al. (2017). The relatively high CO emission in this region may require a reduced conversion factor between OM and CO emissions. The main contribution to PM overestimation of IFS came from the

Geosci. Model Dev. Discuss., https://doi.org/10.5194/gmd-2018-144
Manuscript under review for journal Geosci. Model Dev.
Discussion started: 12 July 2018

night-time values (see next Section). Since night-time overestimation also occurs for NO_2, a lack of vertical mixing during the night in IFS could cause the night time overestimation of the surface values. As already noted, the models tend to underestimate the ozone concentrations, perhaps due to a slight overestimation of the nitrogen oxide concentrations. Another possible explanation is an underestimation of the VOC sources. Routine measurements of VOCs, however, are not available. The need for such measurements, however, needs to be stressed.

The model comparison reported here also shows differences between models in the case of NO, which should probably be attributed to differences in the emissions and emission injection heights of this species and in the formulation of vertical mixing in the boundary layer. Here again, measurements of NO in addition to those of NO_2 and ozone would be useful. Finally, one notes in Figure 9 is the relatively good agreement between models (with the exception of the IFS model) regarding the time evolution of odd oxygen ($Ox = O_3 + NO_2$). The models, however, slightly underestimate the absolute values of the Ox concentration.

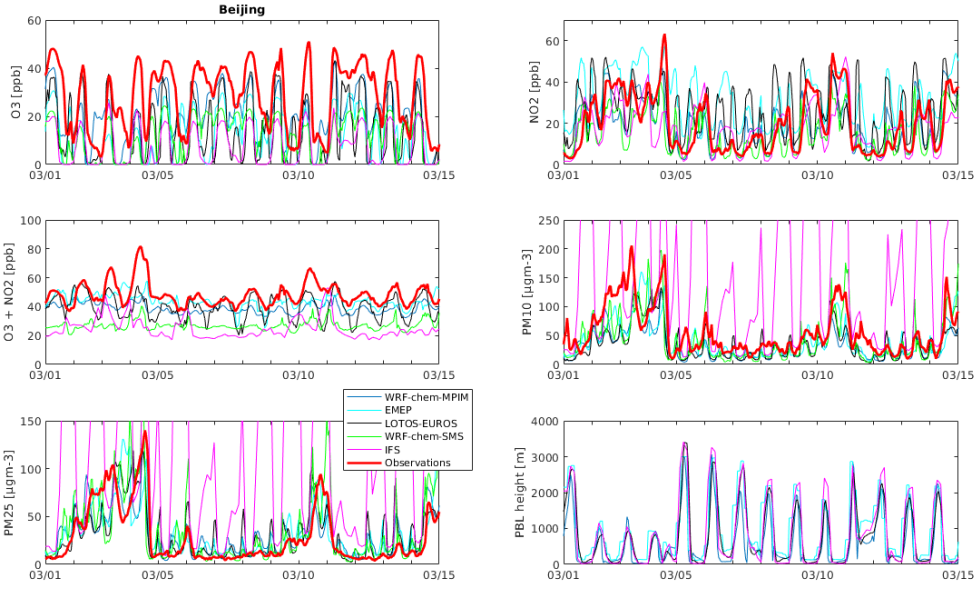

Figure 9. Forecast of the chemical concentrations of ozone, NO_2, PM2.5, and PM10 at Beijing between 1 and 15 March 2017 by the different models involved in the inter-comparison conducted in the present study. The calculated values of $O_x = O_3 + NO_2$ as well as the height of the planetary boundary layer (PBL) are also shown. The mean values from the measurements made at the different monitoring stations of Beijing are shown by the thick red line.

5.5. Diurnal Variations

In order to evaluate the behaviour of the different models regarding their ability to reproduce the diurnal variation in the surface concentrations of ozone, NO_2 and PM2.5, we

have calculated the mean diurnal variations over the period of 1-15 March 2017 averaged for the 34 cities included in our analysis (3 of the 37 cities, located in the western part of the country, and adopted in the MarcoPolo-Panda prediction system have not been considered in this analysis). The resulting results are shown in Figure 10 for ozone and NO_2 (expressed in µg m^{-3}). We have added the corresponding diurnal evolution of Ox (expressed in ppbv) defined as the sum of the ozone and NO_2 mixing ratios. This last chemical variable has the advantage that it is not affected by the fast interchange (null cycle) between ozone and NO_2 by the reactions NO + O_3, NO_2 + hv and O + O_2 +M. Since this cycle tends to transfer "odd oxygen" from ozone to NO_2 after sunset and from NO_2 to ozone after sunrise, the Ox variable is less variable than its two components NO_2 and O_3 over a diurnal cycle. Figure 10 shows that, when averaging over the 34 largest Chinese cities, the diurnal variation of the ensemble median is in good agreement with the observation in the case of NO_2. In the case of ozone, the median values are somewhat underestimated in late morning and in the afternoon. A similar situation is found in the case of Ox. The RMSE for ozone and NO_2, also shown on the figure, is generally lower in the case of the ensemble median than for the individual models. In the case of PM2.5, however, the RMSE of two models, CHIMERE and IFS are smaller than the RMSE of the ensemble median (not shown here). The mean bias of the ensemble median for NO_2 and ozone is generally smaller than that of the individual models. In the case of Ox, some models exhibit a positive bias (WRF-Chem SMS), while others (e.g. SILAM) are characterized by a negative bias.

Figures 11. a, b, c show similar estimates of the diurnal variation in the three large cities of China: Beijing, Shanghai and Guangzhou. These graphs show that the ozone forecast from the ensemble median is lower than observed values during the entire day both in Beijing and in Shanghai. In Guangzhou, however, ozone is slightly overestimated by the prediction. In the case of NO_2, the surface concentrations are overestimated in Beijing and to a lesser extent in Shanghai, with the largest over-prediction occurring during night-time, when the planetary boundary layer is very thin and vertical mixing almost shut off. At the same time, ozone is negatively biased due to its efficient titration by NO_x. In the three cities, the RMSE of NO_2, ozone and Ox appear to be largest at sunset. Thus, a general issue with the MarcoPolo-Panda prediction system is the overestimation of surface NO_2 and the underestimation of ozone concentrations during night-time.

In the case of PM2.5, one of the models involved (IFS) strongly overestimates the concentrations during night-time, but is in fair agreement with observations during daytime. This issue may again reflect a problem with the formulation of species dispersion in the planetary boundary layer. It may also be due to the lack of specified diurnal variation in the emission of primary pollutants as well as to the increased night-time stability.

Geosci. Model Dev. Discuss., https://doi.org/10.5194/gmd-2018-144
Manuscript under review for journal Geosci. Model Dev.
Discussion started: 12 July 2018

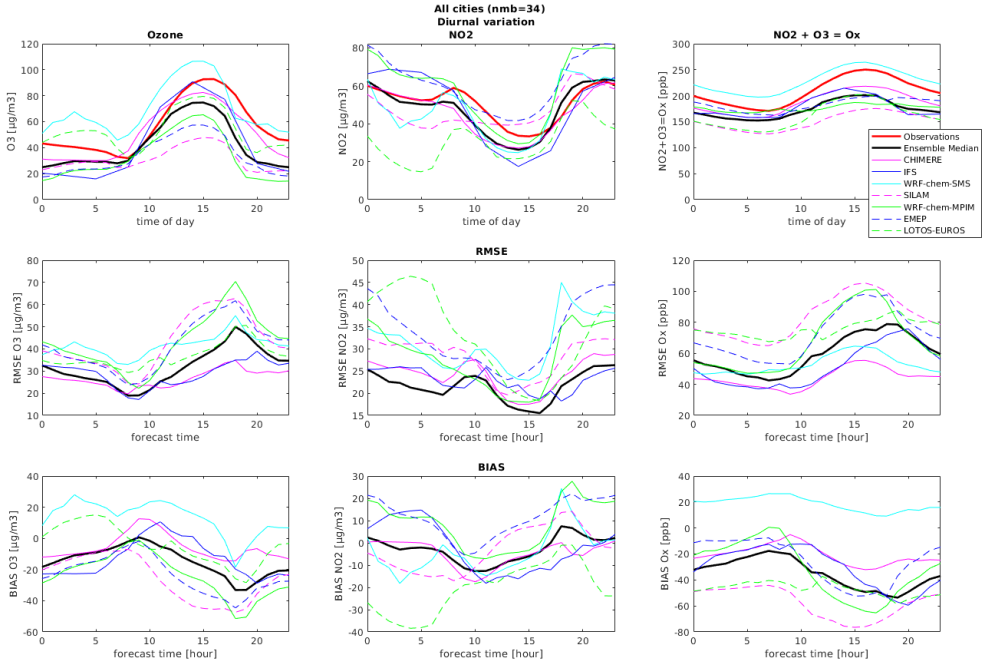

Figure 10. Upper panel: Diurnal variation of ozone (left), NO_2 (middle) and Ox = NO_2 + O_3 (right) for the period 1st - 15th March 2017 for all cities included in the MarcoPolo-Panda Prediction system for all seven models and the ensemble median, and the observations (red line). Middle panel: Root Mean Square Error (RMSE) for ozone (left), NO_2 (middle) and Ox (right). Lower panel: Bias for ozone (left), NO_2 (middle) and Ox (right) for all models and for the ensemble median (black line).

Geosci. Model Dev. Discuss., https://doi.org/10.5194/gmd-2018-144
Manuscript under review for journal Geosci. Model Dev.
Discussion started: 12 July 2018

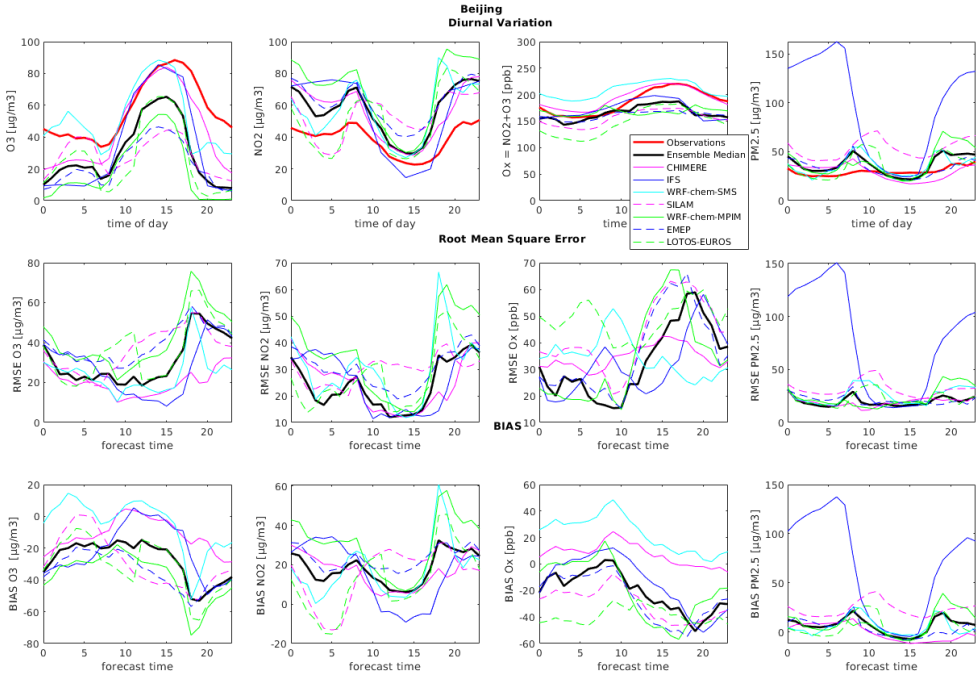

Figure 11.a. Same as Figure 10, but for the urban area of Beijing. The statistical variables for PM2.5 are also included.

Geosci. Model Dev. Discuss., https://doi.org/10.5194/gmd-2018-144
Manuscript under review for journal Geosci. Model Dev.
Discussion started: 12 July 2018

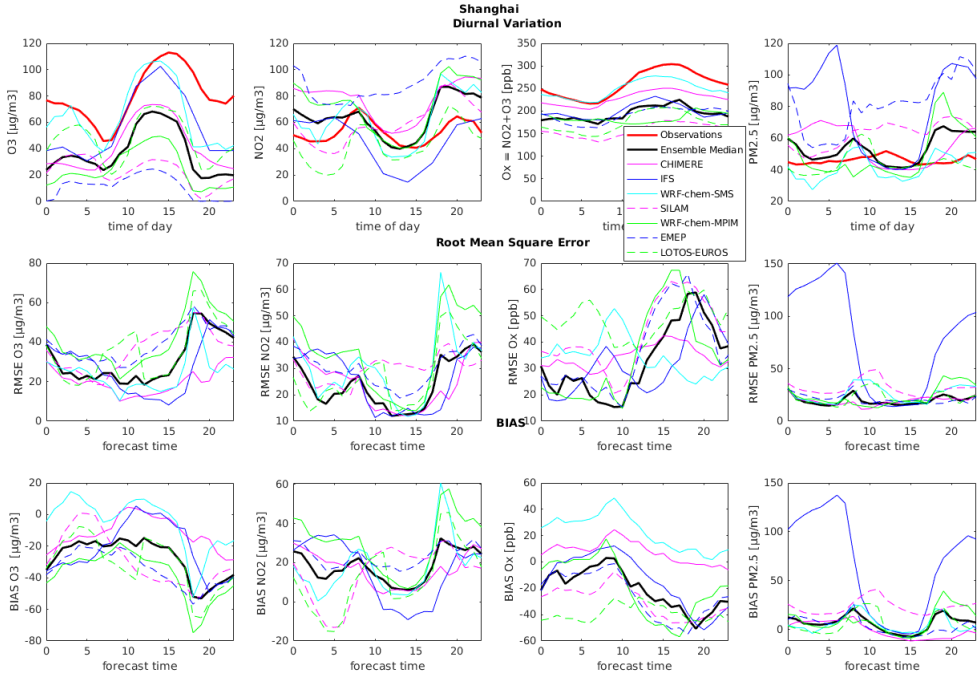

Figure 11b. Same as Figure 10, but for the urban area of Shanghai. The statistical variables for PM2.5 are also included.

Geosci. Model Dev. Discuss., https://doi.org/10.5194/gmd-2018-144
Manuscript under review for journal Geosci. Model Dev.
Discussion started: 12 July 2018

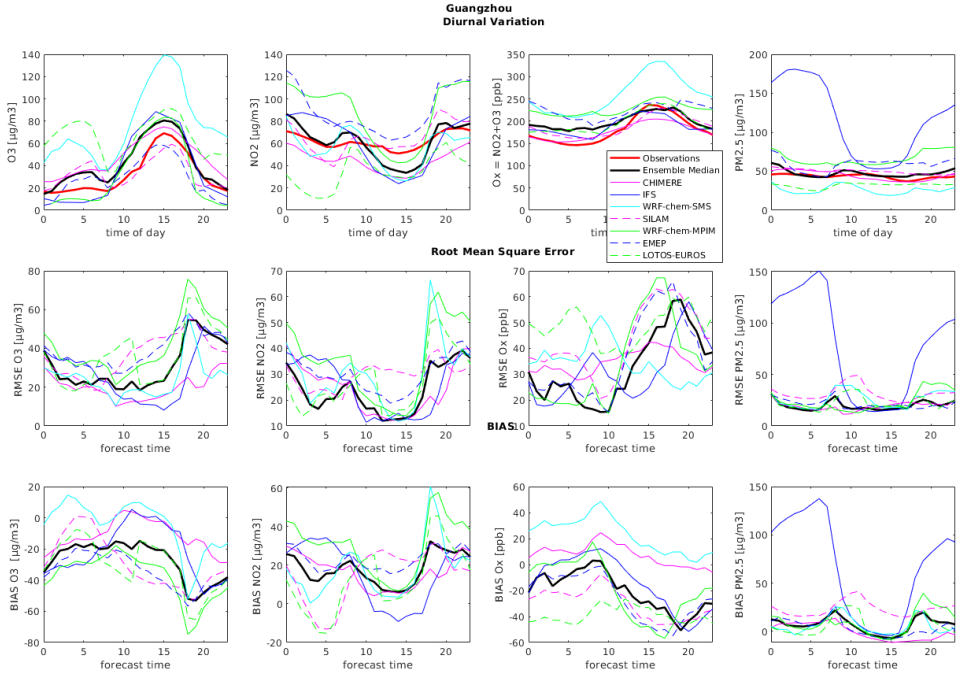

Figure 11c. Same as Figure 10, but for the urban area of Guangzhou. The statistical variables for PM2.5 are also included.

6. Approaches to Improve the Forecasts

The inter-comparison presented in the previous sections provides useful information and represents the basis on which the accuracy of the model predictions can be improved. Since the models have been developed rather independently and the choices about input parameters such as emissions, chemical schemes and adopted weather forecasts have been based on best judgement by these individual teams, a statistical treatment of the model results (e.g., determination of averages and standard deviation) provides in general more reliable information than the data provided by the individual model components of the ensemble. The examination of the model output reveals, however, some systematic biases that could be reduced by identifying the likely cause of these errors.

A simple approach is to recognize that the failure of models to correctly predict air quality could result from several factors: (1) errors in the adopted emissions and the formulation of boundary layer dispersion best diagnosed by analysing the ability of the model to reproduce the monthly mean surface concentrations of chemical species; (2) errors or omission in the adopted chemical scheme leading to inaccuracies in the calculated mean diurnal variations in the concentrations of secondary species; and (3) inaccuracies in the adopted weather forecasts leading to poorly calculated day-to-day variations in the calculated chemical fields. In this later case, one should distinguish between fundamental model biases (i.e., the representation of PBL mixing, a bias that is intrinsic to the models) and the increasing error

in the forecast of synoptic weather patterns as the model integration proceeds. This probably provides an oversimplified view of the causes of errors in chemical weather forecasts, but it offers a simple approach to address some issues in the models and hence to improve the predictions.

A first step towards the improvement of the different model components will be to conduct additional simulations by adopting the same best available emissions data and the same meteorological forecasts. Remaining differences between the models will be due in large part (although not exclusively) to the adopted chemical scheme and the formulation of boundary layer processes. An additional step would be to bring the different formulations of chemistry closer together by at least harmonizing the adopted rate constants and using the same module to calculate photodissociation rates. Finally, it would be interesting to assess the differences in chemical weather predictions resulting from the adopted meteorological forecasts. In particular, it would be important to better constraint the differences in the photolysis rates resulting from the adopted or calculated concentrations of aerosols and in cloudiness. One single model could be run for several days with the weather predictions produced by different meteorological centres.

Finally, a few specific issues from the present inter-comparison require attention:

(1) Most models overestimate the surface levels of NO_2 and PM2.5 as well as other species emitted at the surface, specifically during night-time. The largest discrepancies appear around 18”00 LT when the surface cools and the boundary layer collapses and the emitted species remain trapped in the lowest model layers. Evidently, these models underestimate the vertical exchanges between layers probably produced by the turbulence thermally or mechanically generated by the presence of buildings. Such effects are not accounted for in models that do include a specialized urban formulation. The overestimation of NO_2 during night-time leads to the titration of ozone near the surface and hence an underestimation of the concentration of this gas. The emission injection height is also a relevant factor here, which can largely influence results. During night-time emissions from stacks may be emitted above the mixing layer. However if the injection height in the model is put at lower altitude (or even at the surface) this could lead to overestimation of emissions. The LOTOS-EUROS model evaluated the impact of emission injection heights. An update of the emission heights was tested that injects emissions from industry at lower heights, representing that the number of high stacks is limited (not that contrarily to most models, in the case of LOTOS-EUROS the concentrations at night-time are often underestimated (see Figures 10 and 11). Figure 12 shows diurnal cycles of the simulated PM2.5 concentrations in the city of Chengdu, averaged over an entire year. The updated emission heights clearly have a large (positive) impact on the simulations.
(2) Daytime concentrations of ozone are generally underestimated in most regions of eastern China, even when the level of NO_2 is in reasonable agreement with the values reported by the monitoring stations. The discrepancy could be caused by an underestimation of the emissions of some VOCs, especially in urban areas where ozone is often VOC-limited. More work is required to investigate this question.

Geosci. Model Dev. Discuss., https://doi.org/10.5194/gmd-2018-144
Manuscript under review for journal Geosci. Model Dev.
Discussion started: 12 July 2018

(3) Emissions of primarily pollutants are changing extremely rapidly in China. The adopted emissions inventories usually reflect to the situation a few years before present-day. Since the current emissions have decreased significantly in some urban areas of China in response to measures taken by the authorities, the emissions used in this case for current forecasts may be overestimated. For example, the EMEP model team applied a reduction in NOx emissions after the study period of March 2017 and thereby, through less ozone titration, reduced the severe underestimation of ozone.

(4) Land-use data. Due to the rapid development occurring in particular in the Eastern part of China, land-use data and vegetation change rapidly, and data sets in the model may not accurately reflect the current situation. This has an influence on emissions (including biogenic) but also deposition of pollutants and even meteorology. Land-use data should be updated using satellite observations, urban planning maps and other data sources.

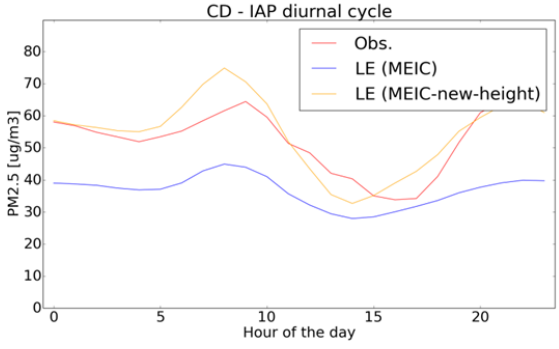

Figure 12. Annually averaged diurnal evolution of the PM2.5 concentrations in the city of Chengdu simulated for different values of the particulate injection height.

7. Conclusions

An operational multi-model air quality forecast system has been established through a close cooperation between European and Chinese research groups and with the support of the European Commission (7th Framework Programme). This system provides daily forecasts for the surface concentration of key pollutants in eastern China, and particularly in the major urban centres of the country. These predictions are posted on a dedicated website (www.marcopolo-panda.eu), where they are compared hour by hour to surface measurements for each city, performed at the monitoring stations deployed in China by the PM2.5 network (www.pm25.int).

The discussions presented in this paper show that in most cases, the model ensemble reproduces quite satisfactorily the synoptic behaviour and the day-to-day variability of the concentrations of ozone and particulate matter and, in particular, predicts the development of most air pollution episodes a few days before their occurrence. This must be attributed to the quality of the weather forecasts at the synoptic scales that are used for the calculation

of chemical species. Overall and in spite of some discrepancies that have been highlighted in the previous sections, the forecast system can therefore be regarded as successful.

The system is in its early phase of development and the purpose of the inter-comparison exercise presented here was to diagnose differences between models and perhaps identify errors. An important objective was to determine ways by which the models could be improved. Even though, in many instances, the surface concentrations are in good or fair agreement with the measured values, differences between calculated and observed values can occasionally be substantial. These occasional differences are often attributed to inaccuracies in the weather forecasts for specific days, but errors in the adopted surface emissions and PBL exchanges or the simplifications introduced in the adopted chemical and aerosol schemes can also be substantial.

The degree by which the concentrations derived by global and regional models, even at high spatial resolution, can be compared with local measurements made in a complex urban canopy remains an important issue that requires further investigation. The insertion of more detailed land-use modules or of a large eddy simulation system in the chemical transport models should be considered in future studies.

Data Availability

The models described here are used operationally by the participating research and service organizations involved in the present study. The data produced by the multi-model forecasting system are available from the Royal Dutch Meteorological Institute (KNMI). The source codes of the modeling systems can be downloaded from the following websites: WRF-Chem: http://www2.mmm.ucar.edu/wrf/users/downloads.html, Chimere: http://www.lmd.polytechnique.fr/chimere/, Silam: http://silam.fmi.fi/, LOTOS-EUROS: https://lotos-euros.tno.nl/, EMEP: http://www.emep.int/, WRF-CMAQ: https://www.epa.gov/cmaq/cmaq-models-0, CMAQ: https://github.com/USEPA/CMAQ/

Acknowledgements

The model inter-comparison presented in the present study has been conducted during a workshop organized in May 2017 by the Shanghai Meteorological Service (SMS) in China. The authors thank Jianming Xu for hosting this meeting and providing support to the participants. The ensemble of models described here has been produced under the Panda and MarcoPolo projects supported by the European Commission within the Framework Program 7 (FP7) under grant agreements n°606719 and n°606953. The National Center for Atmospheric Research (NCAR) is sponsored by the US National Science Foundation.

References

Appel, K. W., Napelenok, S. L., Foley, K. M., Pye, H. O. T., Hogrefe, C., Luecken, D. J. et al..: Overview and evaluation of the Community Multiscale Air Quality (CMAQ) model version 5.1, *Geosci. Model Dev.*, doi:10.5194/gmd-10-1703-2017, 2017.

Bauer, P., A. Thorpe and G. Brunet, The quiet revolution of numerical weather prediction, *Nature*, *525*, 47–55, 2015.

Bergström, R., Denier van der Gon, H. A. C., Prévôt, A. S. H., Yttri, K. E., and Simpson, D.: Modelling of organic aerosols over Europe (2002–2007) using a volatility basis set (VBS) framework: application of different assumptions regarding the formation of secondary organic aerosol, *Atmos. Chem. Phys., 12,* 8499-8527, https://doi.org/10.5194/acp-12-8499-2012, 2012.

Byun, D. and Schere, K. L.: Review of the governing equations, computational algorithms, and other components of the Models-3 Community Multiscale Air Quality (CMAQ) modeling system, *Appl. Mech. Rev., 59*, 51–77, 2006.

Carlton, A. G., Bhave, P. V., Napelenok, S. L., Edney, E. O., Sarwar, G., Pinder, R. W., Pouliot, G. A., and Houyoux, M.: Model Representation of Secondary Organic Aerosol in CMAQv4.7, *Environ. Sci. Technol., 44*, 8553–8560, 2010.

Chang, J.S., Binkowski, F.S., Seaman, N.L., McHenry, J.N., Samson, P.J., Stockwell, W.R., Walcek, C.J., Madronich, S., Middleton, P.B., Pleim, J.E., Lansford, H.H., The regional acid deposition model and engineering model. State-of-Science/Technology, Report 4, National Acid Precipitation Assessment Program, Washington, DC, 1989.

Chen, F., and Dudhia, J.: Coupling an advanced land-surface/hydrology model with the Penn State/NCAR MM5 modeling system. Part I: Model description and implementation. *Mon. Wea. Rev., 129*, 569–585, 2001.

Crippa, M., Janssens-Maenhout, G., Dentener, F., Guizzardi, D., Sindelarova, K., Muntean, M., Van Dingenen, R., and Granier, C.: Forty years of improvements in European air quality: regional policy-industry interactions with global impacts, Atmos. Chem. Phys., 16, 3825-3841, https://doi.org/10.5194/acp-16-3825-2016, 2016.

Dabberdt, W. F., Miller, E., Uncertainty, ensembles and air quality dispersion modeling: applications and challenges, *Atmos. Environ., 34*, 4667-4673, 2000.

Donahue, N. M., A. L. Robinson, C. O. Stanier, and, and S. N. Pandis Coupled Partitioning, Dilution, and Chemical Aging of Semivolatile Organics, *Environmental Science & Technology 40* (8), 2635-2643, DOI: 10.1021/es052297c 2006.

Emmons, L. K., S. Walters, P. G. Hess, J.-F. Lamarque, G. G. Pfister, D. Fillmore, C. Granier, A. Guenther, D. Kinnison, T. Laepple, J. Orlando, X. Tie, G. Tyndall, C. Wiedinmyer, S. L. Baughcum, and S. Kloster, Description and evaluation of the Model for Ozone and Related chemical Tracers, version 4 (MOZART-4), *Geosci. Model Dev., 3,* 43-67, doi:10.5194/gmd-3-43-2010, 2010.

Fast, J. D., W. I. Gustafson, R.C. Easter, R.A. Zaveri, J.C. Barnard, E.G. Chapman, G.A. Grell, and S. E. Peckham, Evolution of ozone, particulates, and aerosol direct radiative forcing in the vicinity of Houston using a fully coupled meteorology-chemistry-aerosol model, *J. Geophys. Res., 111*, D21305, doi:10.1029/2005JD006721, 2006.

Flemming, J., V. Huijnen, J. Arteta, P. Bechtold, A. Beljaars, A.-M. Blechschmidt, A.-M. Diamantakis , R. Engelen, A. Gaudel, A. Inness, L. Jones, B. Josse, E. Katragkou, V. Marecal, V.-H. Peuch, A.

Richter, M.G. Schultz, O. Stein and A. Tsikerdekis, Tropospheric Chemistry in the Integrated Forecasting System of ECMWF, *Geophys. Mod. Dev., 8,* 975-1003, doi:10.5194/gmd-8-975-2015, 2015.

Foley, K. M., Roselle, S. J., Appel, K. W., Bhave, P. V., Pleim, J. E., Otte, T. L., Mathur, R., Sarwar, G., Young, J. O., Gilliam, R. C., Nolte, C. G., Kelly, J. T., Gilliland, A. B., and Bash, J. O.: Incremental testing of the Community Multiscale Air Quality (CMAQ) modeling system version 4.7, *Geosci. Model Dev.*, 3, 205-226, doi:10.5194/gmd-3-205-2010, 2010.

Fountoukis, C., Nenes, A., ISORROPIA II: A Computationally Efficient Aerosol Thermodynamic Equilibrium Model for K^+, Ca^{2+}, Mg^{2+}, NH_4^+, Na^+, SO_4^{2-}, NO_3^-, Cl^-, H_2O Aerosols. *Atmos. Chem. Phys., 7*, 4639-4659, 2007.

Galmarini, S., Kioutsioukis, I., and Solazzo, E.: E pluribus unum*: ensemble air quality predictions, *Atmos. Chem. Phys., 13*, 7153–7182, doi:10.5194/acp-13-7153-2013, 2013.

Ginoux, P., Chin, M., Tegen, I., Prospero, J. M., Holben, B., Dubovik, O., and S.-J. Lin: Sources and distributions of dust aerosols simulated with the GOCART model, *J. Geophys. Res., 106*(D17), 20255–20273, 2001.

Granier, C., B. Bessagnet, T. Bond, A. D'Angiola, H. Denier van der Gon, G. Frost, A. Heil, J. Kaiser, S. Kinne, Z. Klimont, J.-F. Lamarque, C. Liousse, T. Masui, F. Meleux, A. Mieville, T. Ohara, K. Riahi, M. Schultz, S. Smith, A. M. Thomson, J. van Aardenne, and G. van der Werf, Evolution of anthropogenic and biomass burning emissions at global and regional scales during the 1980-2010 period, *Climatic Change,* doi 10.1007/s10584-011-0154-1, 2011.

Grell, G. A., Peckham, S. E., McKeen, S., Schmitz, R., Frost, G., Skamarock, W. C., and Eder, B.: Fully coupled "online" chemistry within the WRF model, *Atmosph. Env., 39*, 6957–6975, 2005.

Grell, G.A., Peckham, S.E., Schmitz, R., McKeen, S.A., Frost, G., Skamarock, W.C. Eder, B., Fully coupled 'online' chemistry in the WRF model. *Atmos. Environ., 39*, 6957-6976, 2005.

Guenther, A. B., Jiang, X., Heald, C. L., Sakulyanontvittaya, T., Duhl, T., Emmons, L. K., and Wang, X.: The Model of Emissions of Gases and Aerosols from Nature version 2.1 (MEGAN2.1): an extended and updated framework for modeling biogenic emissions, *Geosci. Model Dev., 5*, 1471-1492, doi:10.5194/gmd-5-1471-2012, 2012.

Guenther, A., Karl, T., Harley, P., Wiedinmyer, C., Palmer, P. I., and Geron, C.: Estimates of global terrestrial isoprene emissions using MEGAN (Model of Emissions of Gases and Aerosols from Nature), *Atmos. Chem. Phys., 6,* 3181–3210, doi:10.5194/acp-6-3181-2006, 2006

Guenther, A., Zimmerman, P., Wildermuth, M., Natural volatile organic compound emission rate estimates for US woodland landscapes. *Atmos. Environ., 28,* 1197-1210, 1994.

Hong, S.-Y., Noh, Y., and Dudhia, J.: A new vertical diffusion package with an explicit treatment of entrainment processes. *Mon. Wea. Rev., 134,* 2318–2341, 2006.

Hodzic, A. and Jimenez, J. L.: Modeling anthropogenically controlled secondary organic aerosols in a megacity: a simplified framework for global and climate models, *Geosci. Model Dev., 4*, 901-917, doi:10.5194/gmd-4-901-2011, 2011.

Huijnen, V., Williams, J., van Weele, M., van Noije, T., Krol, M., Dentener, F., Segers, A., Houweling, S., Peters, W., de Laat, J., Boersma, F., Bergamaschi, P., van Velthoven, P., Le Sager, P., Eskes, H., Alkemade, F., Scheele, R., Nédélec, P., and Pätz, H.-W., The global chemistry transport model TM5: description and evaluation of the tropospheric chemistry version 3.0, *Geosci. Model Dev.*, *3*, 445-473, doi:10.5194/gmd-3-445-2010, 2010.

Inness, A., A. Blechschmidt, I. Bouarar, S. Chabrillat, M. Crepulja, R. J. Engelen, Q. Errera, J. Flemming, A. Gaudel, V. Huijnen, L. Jones, J. Kapsomenakis, A. Keppens, J.-C. Lambert, B.

1278 Langerock, V.-H. Peuch, M. Razinger, A. Richter, M. G. Schultz, M. Suttie, V. Thouret, M.
1279 Vrekoussis, A. Wagner, and C. Zerefos, Data assimilation experiments with the Composition IFS
1280 developed in the MACC project, *Atmos. Chem. Phys.*, *15,* 5275-5303, doi:10.5194/acp-15-5275-
1281 2015, 2014.

1282 Janssens-Maenhout, G., Crippa, M., Guizzardi, D., Dentener, F., Muntean, M., Pouliot, G., Keating, T.,
1283 Zhang, Q., Kurokawa, J., Wankmüller, R., Denier van der Gon, H., Kuenen, J. J. P., Klimont, Z.,
1284 Frost, G., Darras, S., Koffi, B., and Li, M.: HTAP_v2.2: a mosaic of regional and global emission
1285 grid maps for 2008 and 2010 to study hemispheric transport of air pollution, *Atmos. Chem.*
1286 *Phys., 15*, 11411-11432, doi:10.5194/acp-15-11411-2015, 2015.

1287 Kouznetsov, R., Sofiev, M.: A methodology for evaluation of vertical dispersion and dry deposition of
1288 atmospheric aerosols, *J. Geophys. Res*, 117, 2012.

1289 Kukkonen, J., Olsson, T., Schultz, D. M., Baklanov, A., Klein, T., Miranda, A. I., Monteiro, A., Hirtl, M.,
1290 Tarvainen, V., Boy, M., Peuch, V.-H., Poupkou, A., Kioutsioukis, I., Finardi, S., Sofiev, M., Sokhi,
1291 R., Lehtinen, K. E. J., Karatzas, K., San José, R., Astitha, M., Kallos, G., Schaap, M., Reimer, E.,
1292 Jakobs, H. and Eben, K.: A review of operational, regional-scale, chemical weather forecasting
1293 models in Europe, *Atmos. Chem. Phys., 12*, 1–87, doi:10.5194/acp-12-1-2012, 2012.

1294 Li, M., Zhang, Q., Streets, D., He, K.B., Cheng, Y.F., Emmons, L. K., Huo, H., Kang, S.C., Lu, Z., Shao, M.,
1295 Su, H., Yu, X., Zhang, Y., Mapping Asian anthropogenic emissions of non-methane volatile
1296 organic compounds to multiple chemical mechanisms, *Atmos. Chem. Phys., 14*, 5617-5638,
1297 2014.

1298 Li, M., Zhang, Q., Kurokawa, J.-I., Woo, J.-H., He, K., Lu, Z., Ohara, T., Song, Y., Streets, D. G.,
1299 Carmichael, G. R., Cheng, Y., Hong, C., Huo, H., Jiang, X., Kang, S., Liu, F., Su, H., and Zheng, B.:
1300 MIX: a mosaic Asian anthropogenic emission inventory under the international collaboration
1301 framework of the MICS-Asia and HTAP, *Atmos. Chem. Phys., 17,* 935-963,
1302 https://doi.org/10.5194/acp-17-935-2017, 2017.

1303 Liu, F., Zhang, Q., Tong, D., Zheng, B., Li, M., Huo, H., He, K.B., High-resolution inventory of
1304 technologies, activities, and emissions of coal-fired power plants in China from 1990 to 2010,
1305 *Atmos. Chem. Phys., 15*(13), 18787-18837, 2015.

1306 Lorenc, A.C, A global three-dimensional multivariate statistical interpolation scheme, *Mon. Wea.*
1307 *Rev., 109*, 701- 721, 1981

1308 Madronich, S., Flocke, S., The role of solar radiation in atmospheric chemistry. Boule P. (Ed.),
1309 *Handbook of Environmental Chemistry*. Springer, Heidelberg, 1999.

1310 Manders, A. M. M., Builtjes, P. J. H., Curier, L., Denier van der Gon, H. A. C., Hendriks, C., Jonkers, S.,
1311 Kranenburg, R., Kuenen, J., Segers, A. J., Timmermans, R. M. A., Visschedijk, A., Wichink Kruit, R.
1312 J., Van Pul, W. A. J., Sauter, F. J., van der Swaluw, E., Swart, D. P. J., Douros, J., Eskes, H., van
1313 Meijgaard, E., van Ulft, B., van Velthoven, P., Banzhaf, S., Mues, A., Stern, R., Fu, G., Lu, S.,
1314 Heemink, A., van Velzen, N., and Schaap, M., *Curriculum Vitae of the LOTOS-EUROS (v2.0)*
1315 *chemistry transport model*, *Geosci. Model Dev.*, doi:10.5194/gmd-2017-88, 2017

1316 Marécal, V., Peuch, V.-H., Andersson, C., Andersson, S., Arteta, J., Beekmann, M., Benedictow, A.,
1317 Bergström, R., et al.: A regional air quality forecasting system over Europe: the MACC-II daily
1318 ensemble production, *Geosci. Model Dev., 8*, 2777–2813, doi:10.5194/gmd-8-2777-2015, 2015.

1319 Menut L, B.Bessagnet, D.Khvorostyanov, M.Beekmann, N.Blond, A.Colette, I.Coll, G.Curci, G.Foret,
1320 A.Hodzic, S.Mailler, F.Meleux, J.L.Monge, I.Pison, G.Siour, S.Turquety, M.Valari, R.Vautard and
1321 M.G.Vivanco, 2013, CHIMERE 2013: a model for regional atmospheric composition modelling,
1322 *Geoscientific Model Development, 6,* 981-1028, doi:10.5194/gmd-6-981-2013a

1323 Menut, L., Perez Garcia-Pando, C., Haustein, K., Bessagnet, B., Prigent, C., and Alfaro, S.: Relative
1324 impact of roughness and soil texture on mineral dust emission fluxes modeling, *J. Geophys.*
1325 *Res., 118,* 6505–6520, doi:10.1002/jgrd.50313, 2013b

1326 Monahan E.C., Spiel D.E., Davidson K.L., A Model of Marine Aerosol Generation Via Whitecaps and
1327 Wave Disruption. In: Monahan E.C., Niocaill G.M. (eds) Oceanic Whitecaps. Oceanographic
1328 Sciences Library, vol 2. Springer, Dordrecht, 1986.

1329 Morcrette, J.-J., Boucher, O., Jones, L., Salmond, D. , Bechtold, P., Beljaars, A., Benedetti, A., Bonet,
1330 A., Kaiser, J. W., Razinger, M., Schulz, M. , Serrar, S. , Simmons, A. J., Sofiev, M., Suttie, M.,
1331 Tompkins, A. M. and Untch, A.: Aerosol analysis and forecast in the ECMWF Integrated Forecast
1332 System. Part I: Forward modelling, *J. Geophys. Res.*, 2009.

1333 Muntean, M, G. Janssens-Maenhout, S. Song, N.E. Selin, J.G.J. Olivier, D. Guizzardi, R. Maas, F.
1334 Dentener, 2014, Trend analysis from 1970 to 2008 and model evaluation of EDGARv4 global
1335 gridded anthropogenic mercury emissions, *Science of the Total Environment*, Vol. 494–495, 1
1336 Oct.2014, pp. 337–350
1337 (http://www.sciencedirect.com/science/article/pii/S0048969714008572)

1338 Nenes, A., Pilinis, C., and Pandis, S.: ISORROPIA: A new thermodynamic model for inorganic
1339 multicomponent atmospheric aerosols, *Aquat. Geochem., 4,* 123–152, 1998.

1340 Poupkou, A., Giannaros, T., Markakis, K., Kioutsioukis, I., Curci, G., Melas, D., and Zerefos, C.: A
1341 model for European Biogenic Volatile Organic Compound emissions: Software development
1342 and first validation, *Environ. Modell. Softw.*, 25, 1845–1856, 2010.

1343 Riccio, A., Giunta, G., and Galmarini, S.: Seeking for the rational basis of the Median Model: the
1344 optimal combination of multimodel ensemble results, *Atmos. Chem. Phys., 7*, 6085–6098,
1345 doi:10.5194/acp-7-6085-2007, 2007.

1346 Schell, B., Ackermann, I., Hass, H., et al., Modeling the formation of secondary organic aerosol within
1347 a comprehensive air quality model system. *J. Geophys. Res., 106,* 28275-28293, 2001.

1348 Shrivastava, M., Fast, J., Easter, R., Gustafson Jr., W. I., Zaveri, R. A., Jimenez, J. L., Saide, P., and
1349 Hodzic, A.: Modeling organic aerosols in a megacity: comparison of simple and complex
1350 representations of the volatility basis set approach, *Atmos. Chem. Phys.*, *11*, 6639-6662, 2011.

1351 Simpson, D., Benedictow, A., Berge, H., Bergström, R., Emberson, L. D., Fagerli, H., Flechard, C. R.,
1352 Hayman, G. D., Gauss, M., Jonson, J. E., Jenkin, M. E., Nyíri, A., Richter, C., Semeena, V. S., Tsyro,
1353 S., Tuovinen, J.-P., Valdebenito, Á., and Wind, P.: The EMEP MSC-W chemical transport model –
1354 technical description, *Atmos. Chem. Phys., 12*, 7825-7865, doi:10.5194/acp-12-7825-2012,
1355 2012.

1356 Simpson, D., Nyri, A., Tsyro, S., Valdebenito, Á., and Wind, P.: Updates to the EMEP/MSC-W model,
1357 2015-2016 Transboundary particulate matter, photo-oxidants, acidifying and eutrophying
1358 components. EMEP Status Report 1/2016, The Norwegian Meteorological Institute, Oslo,
1359 Norway, 2016, 133-139, ISSN 1504-6109, 2016.

1360 Simpson, D., Tsyro, S., and Wind, P.: Updates to the EMEP/MSC-W model, Transboundary particulate
1361 matter, photo-oxidants, acidifying and eutrophying components. EMEP Status Report 1/2015,
1362 The Norwegian Meteorological Institute, Oslo, Norway, 2015, 129-138, ISSN 1504-6109, 2015.

1363 Skamarock, W. C., and Coauthors, A description of the Advanced Research WRF version 3. NCAR
1364 Tech. Note NCAR/TN-4751 STR, 125 pp.
1365 [http://www2.mmm.ucar.edu/wrf/users/docs/arw_v3.pdf], 2008.

1366 Soares, J., Sofiev, M., Hakkarainen, J.: Uncertainties of wild-land fires emission in AQMEII phase 2
1367 case study. *Atmosph.Environ., 115,* 361-370, 2015.

1368 Sofiev M, Kouznetsov R, Prank M, Soares Alves Antunes J, Vira J, Tarvainen V.: A long-term re-
1369 analysis of atmospheric composition and air quality. ITM 35, 2016.

1370 Sofiev, M., Genikhovich, E., Keronen, P., Vesala, T.: Diagnosing the surface layer parameters for
1371 dispersion models within the meteorological-to-dispersion modeling interface, *J. of Appl.*
1372 *Meteorol. and Climatology*, *49*, 221-233, 2010.

1373 Sofiev, M., Soares, J., Prank, M., de Leeuw, G., Kukkonen, J.: A regional-to-global model of emission
1374 and transport of sea salt particles in the atmosphere. *J. Geophys. Res*, 116, D21302, 4713, 2011.

1375 Sofiev, M., Vira, J., Kouznetsov, R., Prank, M., Soares, J., Genikhovich, E. : Construction of the SILAM
1376 Eulerian atmospheric dispersion model based on the advection algorithm of Michael Galperin,
1377 *Geosci.Model Developm.* 8, 3497-3522, 2015.

1378 Sofiev, M., Berger, U., Prank, M., Vira, J., Arteta, J., Belmonte, J., Bergmann, K.-C., Chéroux, F.,
1379 Elbern, H., Friese, E., Galan, C., Gehrig, R., Khvorostyanov, D., Kranenburg, R., Kumar, U.,
1380 Marécal, V., Meleux, F., Menut, L., Pessi, A.-M., Robertson, L., Ritenberga, O., Rodinkova, V.,
1381 Saarto, A., Segers, A., Severova, E., Sauliene, I., Siljamo, P., Steensen, B. M., Teinemaa, E.,
1382 Thibaudon, M., and Peuch, V.-H. (2015) MACC regional multi-model ensemble simulations of
1383 birch pollen dispersion in Europe, *Atmos. Chem. Phys., 15,* 8115-8130, doi:10.5194/acp-15-
1384 8115-2015, http://www.atmos-chem-phys.net/15/8115/2015/.

1385 Sofiev, M., Ritenberga, O., Albertini, R., Arteta, J., Belmonte, J., Bonini, M., Celenk, S., Damialis, A.,
1386 Douros, J., Elbern, H., Friese, E., Galan, C., Gilles, O., Hrga, I., Kouznetsov, R., Krajsek, K.,
1387 Parmentier, J., Plu, M., Prank, M., Robertson, L., Steensen, B. M., Thibaudon, M., Segers, A.,
1388 Stepanovich, B., Valdebenito, A. M., Vira, J., and Vokou, D.: (2017) Multi-model ensemble
1389 simulations of olive pollen distribution in Europe in 2014, *Atmos. Chem. Phys.,* doi:10.5194/acp-
1390 2016-1189, https://www.atmos-chem-phys.net/17/12341/2017/acp-17-12341-2017.html

1391 Sofiev, M.: A model for the evaluation of long-term airborne pollution transport at regional and
1392 continental scales. *Atmosph. Environ*. 34, 15, 2481-2493, 2000.

1393 Solazzo, E., Bianconi, R., Vautard, R., Appel, K. W., Moran, M. D., Hogrefe, C., Bessagnet, B., Brandt,
1394 J., Christensen, J. H., Chemel, C., Coll, I., Denier van der Gon, H., Ferreira, J., Forkel, R., Francis,
1395 X. V., Grell, 5 G., Grossi, P., Hansen, A. B., Jericevic, A., Kraljevic, L., Miranda, A. I., Nopmongcol,
1396 U., Pirovano, G., Prank, M., Riccio, A., Sartelet, K. N., Schaap, M., Silver, J. D., Sokhi, R. S., Vira,
1397 J., Werhahn, J., Wolke, R., Yarwood, G., Zhang, J., Rao, S. T., and Galmarini, S.: Model evalution
1398 and ensemble modelling of surface-level ozone in Europe and North America in the context of
1399 AQMEII, *Atmos. Environ., 53*, 60–74, 2012.

1400 Spracklen, D. V., Jimenez, J. L., Carslaw, K. S., Worsnop, D. R., Evans, M. J., Mann, G. W., Zhang, Q.,
1401 Canagaratna, M. R., Allan, J., Coe, H., McFiggans, G., Rap, A., and Forster, P.: Aerosol mass
1402 spectrometer constraint on the global secondary organic aerosol budget, Atmos. Chem. Phys.,
1403 11, 12109-12136, https://doi.org/10.5194/acp-11-12109-2011, 2011.

1404 Szopa, S., Foret, G., Menut, L., and Cozic, A.: Impact of large scale circulation on European summer
1405 surface ozone: consequences for modeling, *Atmos. Environ., 43,* 1189–1195,
1406 doi:10.1016/j.atmosenv.2008.10.039, 2009

1407 Thompson, G., Field, P. R., Rasmussen, R.M., and Hall, W.D.: Explicit Forecasts of winter precipitation
1408 using an improved bulk microphysics scheme. Part II: Implementation of a new snow
1409 parameterization. *Mon. Wea. Rev., 136*, 5095–5115, 2008.

1410 Timmermans, R., R. Kranenburg, A. Manders, C. Hendriks, A. Segers, E. Dammers, Q. Zhang, L. Wang,
1411 Z. Liu, L. Zeng, H. Denier van der Gon, M. Schaap, *Source apportionment of PM2.5 across China*
1412 *using LOTOS-EUROS*, *Atmospheric Environment,* 10.1016/j.atmosenv.2017.06.003, 2017

1413 Tie, X., Madronich, S., Walters, S., Rasch, P., Collins, W., Effect of clouds on photolysis and oxidants
1414 in the troposphere. *J. Geophys. Res., 108,* 4642, 2003.

1415 Vautard, R. et al., Is regional air quality model diversity representative of uncertainty for ozone
1416 simulation? *Geophys. Res. Lett., 33,* L24818, doi:10.1029/2006GL027610, 2006.

1417 Wesely, M.: Parameterization of Surface Resistances to Gaseous Dry Deposition in Regional-Scale
1418 Numerical Models, *Atmos. Environ., 23,* 1293–1304, 1989

1419 Wild, O., Fiore, A. M., Shindell, D. T., Doherty, R. M., Collins, W. J., Dentener, F. J., Schultz, M. G.,
1420 Gong, S., MacKenzie, I. A., Zeng, G., Hess, P., Duncan, B. N., Bergmann, D. J., Szopa, S., Jonson, J.
1421 E., Keating, T. J., and Zuber, A.: Modelling future changes in surface ozone: a parameterized
1422 approach, *Atmos. Chem. Phys., 12*, 2037-2054, doi:10.5194/acp-12-2037-2012, 2012.

1423 Wild, O., Zhu, X., and Prather, M. J.: Fast-J: Accurate Simulation of In- and Below-Cloud Photolysis in
1424 Tropospheric Chemical Models, *J. Atmos. Chem., 37*, 245–282, 2000

1425 Yarwood, G., S. Rao, M. Yocke, and G. Whitten.: Updates to the Carbon Bond Chemical Mechanism:
1426 CB05, *Final Report to the U.S. EPA*, RT-04-00675, RTP, NC, 2005.

1427 Zaveri, R. A., Easter, R. C., Fast, J. D., Peters, L. K., Model for Simulating Aerosol Interactions and
1428 Chemistry (MOSAIC), *J. Geophys. Res.*, *113, D13204, doi:*10.1029/2007JD008782, 2008.
1429
1430
1431